

Automatic Personalized Impression Generation for PET Reports Using Large Language Models

Xin Tie^{1,2} MS, Muheon Shin¹ MD, Ali Pirasteh^{1,2} MD, Nevein Ibrahim¹ MD, Zachary Huemann¹ MS, Sharon M. Castellino^{3,4} MD, Kara M. Kelly^{5,6} MD, John Garrett^{1,2} PhD, Junjie Hu^{7,8} PhD, Steve Y. Cho^{1,9} MD, Tyler J. Bradshaw¹ PhD

1. Department of Radiology, School of Medicine and Public Health, University of Wisconsin, Madison, WI, USA

2. Department of Medical Physics, School of Medicine and Public Health, University of Wisconsin, Madison, WI, USA

3. Department of Pediatrics, Emory University School of Medicine, Atlanta, GA, USA

4. Aflac Cancer and Blood Disorders Center, Children's Healthcare of Atlanta, Atlanta, GA, USA

5. Department of Pediatric Oncology, Roswell Park Comprehensive Cancer Center, Buffalo, NY, USA.

6. Department of Pediatrics, University at Buffalo Jacobs School of Medicine and Biomedical Sciences, Buffalo, NY, USA.

7. Department of Biostatistics and Medical Informatics, School of Medicine and Public Health, University of Wisconsin, Madison, WI, USA

8. Department of Computer Science, School of Computer, Data and Information Sciences, University of Wisconsin, Madison, WI, USA

9. University of Wisconsin Carbone Comprehensive Cancer Center, Madison, WI, USA

Address correspondence to:

Tyler J. Bradshaw, Ph.D.,

Department of Radiology, School of Medicine and Public Health,

University of Wisconsin in Madison, Madison, WI 53705,

Email: tbradshaw@wisc.edu

Summary: The fine-tuned large language model provides clinically useful, personalized impressions based on PET findings. To our knowledge, this is the first study to automate impression generation for whole-body PET reports.

Key Points

- Among 30 evaluation metrics, domain-adapted BARTScore and PEGASUSScore exhibited the highest correlations (Spearman's ρ correlation=0.568 and 0.563) with physician preferences, yet they did not reach the level of inter-reader correlation (ρ =0.654).
- Of all fine-tuned large language models, encoder-decoder models outperformed decoder-only models, with PEGASUS emerging as the top-performing model.
- In the reader study, three nuclear medicine physicians considered the overall utility of personalized PEGASUS-generated impressions to be comparable to clinical impressions dictated by other physicians.

Keywords: PET report summarization, Findings, Impressions, Large Language Models, Informatics

Abbreviations:

LLM: Large Language Model

NM: Nuclear Medicine

DS: Deauville score

ROUGE: Recall-Oriented Understudy for Gisting Evaluation

Abstract

Purpose

To determine if fine-tuned large language models (LLMs) can generate accurate, personalized impressions for whole-body PET reports.

Materials and Methods

Twelve language models were trained on a corpus of PET reports using the teacher-forcing algorithm, with the report findings as input and the clinical impressions as reference. An extra input token encodes the reading physician's identity, allowing models to learn physician-specific reporting styles. Our corpus comprised 37,370 retrospective PET reports collected from our institution between 2010 and 2022. To identify the best LLM, 30 evaluation metrics were benchmarked against quality scores from two nuclear medicine (NM) physicians, with the most aligned metrics selecting the model for expert evaluation. In a subset of data, model-generated impressions and original clinical impressions were assessed by three NM physicians according to 6 quality dimensions and an overall utility score (5-point scale). Each physician reviewed 12 of their own reports and 12 reports from other physicians. Bootstrap resampling was used for statistical analysis.

Results

Of all evaluation metrics, domain-adapted BARTScore and PEGASUSScore showed the highest Spearman's ρ correlations (0.568 and 0.563) with physician preferences. Based on these metrics, the fine-tuned PEGASUS model was selected as the top LLM. When physicians reviewed PEGASUS-generated impressions in their own style, 89% were considered clinically acceptable, with a mean utility score of 4.08/5. Physicians rated these personalized impressions as comparable in overall utility to the impressions dictated by other physicians (4.03, $P=0.41$).

Conclusion

Personalized impressions generated by PEGASUS were clinically useful, highlighting its potential to expedite PET reporting.

Introduction

The radiology report serves as the official interpretation of a radiological examination and is essential for communicating relevant clinical findings amongst reading physicians, the healthcare team, and patients. Compared to other imaging modalities, reports for whole-body PET exams (e.g., skull base to thigh or skull vertex to feet) are notable for their length and complexity (1). In a typical PET report, the findings section details numerous observations about the study and the impression section summarizes the key findings. Given that referring physicians primarily rely on the impression section for clinical decision-making and management (2), it is paramount to ensure its accuracy and completeness. However, creating PET impressions that encapsulate all important findings can be time-consuming and error-prone (3). Large language models (LLMs) have the potential to accelerate this process by automatically drafting impressions based on the findings.

While LLMs have been used previously to summarize radiology findings (3–8), impression generation for whole-body PET reports has received comparatively little attention. Unlike general chest x-ray reports that comprise 40-70 words (9) in the findings section, whole-body PET reports often have 250-500 words in the findings section and contain observations across multiple anatomical regions with cross comparison to available anatomic imaging modalities (e.g., CT and MRI) and clinical correlation. This complexity heightens the risk of omissions in the generated impressions. Furthermore, the length of PET impressions can accentuate the unique reporting styles of individual reading physicians, underscoring the need for personalized impression generation. Consequently, adapting LLMs for PET report summarization presents distinct challenges.

Evaluating the performances of LLMs in the task of impression generation is also challenging, given that a single case can have various acceptable impressions. While expert evaluation stands as the gold standard, it is impractical for physicians to exhaustively review outputs of all LLMs to determine the leading model. In recent years, several evaluation metrics designed for general text summarization have been adapted to evaluate summaries of medical documents (10-12). However, it remains unclear how well these metrics could assess the quality of PET impressions and which of them align most closely with physician judgements.

This study aimed to explore whether the LLMs fine-tuned on a large corpus of PET clinical reports can accurately summarize PET findings and generate impressions suitable for clinical use. We benchmarked 30 evaluation metrics against physician preferences and then selected the top-performing LLM. To assess its clinical utility, we conducted an expert reader study, identifying common mistakes made by the LLM. We also investigated the importance of

personalizing impressions for reading physicians. Lastly, we evaluated the model’s reasoning capability within the nuclear medicine (NM) domain.

Materials and Methods

Dataset Collection

Under a protocol approved by the institutional review board and with a waiver of informed consent, we collected 37,370 retrospective PET reports, dictated by 65 physicians, from our institution between January 2010 and January 2023. Appendix S1 presents the statistics of PET reports in our dataset. All reports were anonymized using NLM-Scrubber (13). Of 37,370 PET reports, 4000 were randomly selected for internal testing, 2000 were used for validation, and the remaining 31,370 reports were used for training.

Report Preprocessing

In this work, we investigated both encoder-decoder and decoder-only language models. Considering their different architectures, we customized input formats as illustrated in Figure 1. For encoder-decoder models, the first lines describe the categories of PET scans, while the second lines encode each reading physician’s identity using an identifier token (details in Appendix S2). The “Findings” section contains the clinical findings from the PET reports, whereas the “Indications” section encompasses relevant background information, including the patient’s medical history and the reason for the examination. For decoder-only models, we employed the instruction-tuning method (15) and adapted the prompt from (16). Each case starts with the instruction: “Derive the impression from the given [description] report for [physician].” The PET findings and background information are concatenated to form the “Input” section. The original clinical impressions are used as the reference for model training and evaluation.

Models for PET Report Summarization

We formulated our work as an abstractive summarization task since physicians typically interpret findings in the impression section, rather than merely reusing sentences from the findings section. We fine-tuned 8 encoder-decoder models and 4 decoder-only models, covering a broad range of language models for sequence generation. The encoder-decoder models comprised state-of-the-art (SOTA) transformer-based models, namely BART (17), PEGASUS (18), T5 (19) and FLAN-T5 (20). To investigate if the medical-domain adaptation could benefit our task, we fine-tuned 2 biomedical LLMs, BioBART (21) and Clinical-T5 (22). Additionally, we included 2 baseline models, pointer-generator network (PGN) (3) and BERT2BERT (23).

The decoder-only models encompassed GPT2 (24) and OPT (25) as well as the recently released LLaMA (26) and Alpaca (16). All models were trained using the standard teacher-forcing algorithm. LLaMA and Alpaca were fine-tuned with low-rank adaptation (LoRA) (27) to reduce memory usage and accelerate training, while the other models were subjected to full fine-tuning. We adopted the beam search decoding algorithm to generate impressions. More comprehensive information about these models, including their training and inference settings, can be found in Appendix S3.

Our models are made available on Hugging Face: huggingface.co/xtie/PEGASUS-PET-impression. The code can be found in the open-source project: github.com/xtie97/PET-Report-Summarization.

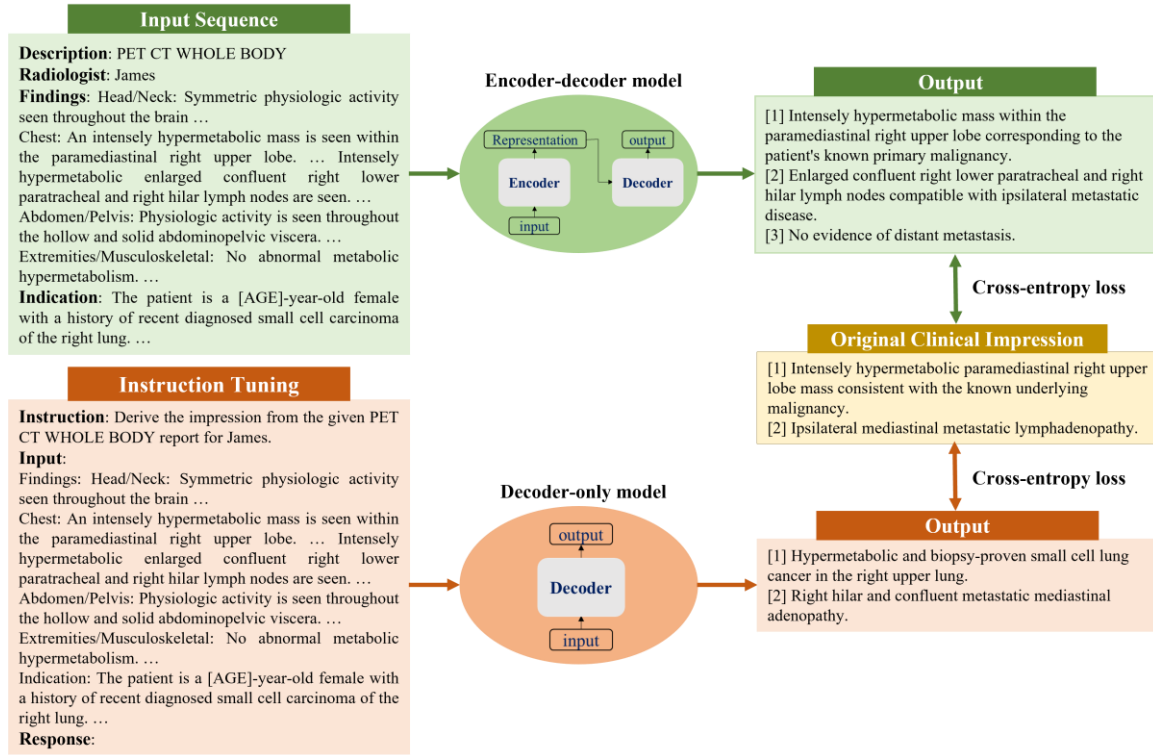


Figure 1: Formatting of reports for input to encoder-decoder and decoder-only models. For encoder-decoder models, the first two lines describe the examination category and encode the reading physician’s identity, respectively. “Findings” contains the clinical findings from the PET report, and “Indication” includes the patient’s medical history and the reason for the examination. For decoder-only models, each case follows a specific format for the instruction: “Derive the impression from the given [description] for [physician]”. “Input” accommodates the concatenation of clinical findings and indications. The output always starts with the prefix “Response:”. Both model architectures utilize the cross-entropy loss to compute the difference between original clinical impressions and model-generated impressions.

Benchmarking Evaluation Metrics

To identify the evaluation metrics most correlated with physician preferences, we presented impressions generated by 4 different models (PGN, BERT2BERT, BART, PEGASUS) to two

NM physicians. These models represented a wide performance spectrum. One physician (M.S.) reviewed 200 randomly sampled reports in the test set, then scored the quality of model-generated impressions on a 5-point Likert scale. The definitions of each level are provided in Appendix S4. To assess inter-observer variability, a second physician (S.Y.C.) independently scored 20 of the cases based on the same criterion.

Table 1 categorizes the evaluation metrics (detailed introductions in Appendix S4) included in this study. To address the domain gap between general-domain articles and PET reports, we fine-tuned BARTScore on our PET reports using the method described in (28) and named it BARTScore+PET. Following the same approach, we developed PEGASUSScore+PET and T5Score+PET. These three evaluators are made available at huggingface.co/xtie/BARTScore-PET. The Spearman’s ρ correlation quantified how well evaluation metrics correlated with the physicians’ judgements. Metrics with the highest correlations were used to determine the top-performing model.

Expert Evaluation:

To examine the clinical utility of our best LLM, we conducted a reader study involving three physicians: two board-certified in NM (N.I., S.Y.C.) and one board-certified in NM and radiology (A.P.). Blinded to the original interpreting physicians, each reader independently reviewed a total of 24 whole-body PET reports along with model-generated impressions. Of these, twelve cases were originally dictated by themselves, and the rest were dictated by other physicians. The LLM impressions were always generated in the style of the interpreting physician by using their specific identifier token. The scoring system included 6 quality dimensions (3-point scale) and an overall utility score (5-point scale). Their definitions are described in Table 2. The platform we designed for physician reviews of test cases can be assessed at xtie97/PET-Report-Expert-Evaluation.

Additional Analysis

To further evaluate the capability of our fine-tuned LLMs, we conducted three additional experiments. Implementation details are provided in Appendix S5:

1. **Deauville score (DS) prediction:** To test the reasoning capability of our models within the NM domain, we classified PET lymphoma reports into DS 1-5 based on the exam-level DSs (29) extracted from model-generated impressions. The original clinical impressions served as the reference for the DSs. The evaluation metrics included the 5-class accuracy and the linearly weighted Cohen’s κ index. For context, our prior study (29) showed that a human expert

achieved 66% accuracy and a Cohen’s κ of 0.79 when the redacted PET reports and maximum intensity projection (MIP) images were given.

2. Encoding physician-specific styles: We compared the impressions generated in the styles of two physicians (Physician 1 and Physician 2) who had distinct reporting styles. Physician 1’s impressions tended to be more detailed, whereas Physician 2’s impressions were more concise.

Statistical analysis

Using bootstrap resampling (30), the 95% confidence intervals (CI) for our results were derived from 10,000 repetitive trials. The difference between two data groups were statistically significant at 0.05 only when one group exceeded the other in 95% of trials.

Table 1: All evaluation metrics included in this study and their respective categories.

Category	Definition	Corresponding Evaluation Metrics
Lexical overlap-based metrics	These metrics measure the overlap between the generated text and the reference in terms of textual units, such as n-grams or word sequences.	ROUGE-1, ROUGE-2, ROUGE-3, ROUGE-L, ROUGE-LSUM, BLEU, CHRF, METEOR, CIDEr
Embedding-based metrics	These metrics measure the semantic similarity between the generated and reference texts using pretrained embeddings.	ROUGE-WE-1, ROUGE-WE-2, ROUGE-WE-3, BERTScore, MoverScore
Graph-based metrics	These metrics construct graphs using entities and their relations extracted from the sentences, and evaluate the summary based on these graphs.	RadGraph
Text generation-based metrics	These metrics assess the quality of generated text by framing it as a text generation task using sequence-to-sequence language models.	BARTScore, BARTScore+PET, PEGASUSScore+PET, T5Score+PET, PRISM
Supervised regression-based metrics	These metrics require human annotations to train a parametrized regression model to predict human judgements for the given text.	S ³ -pyr, S ³ -resp
Question answering-based metrics	These metrics formulate the evaluation process as a question-answering task by guiding the model with various questions.	UniEval
Reference-free metrics	These metrics do not require the reference text to assess the quality of the generated text. Instead, they compare the generated text against the source document.	SummaQA, BLANC, SUPERT, Stats-compression, Stats-coverage, Stats-density, Stats-novel trigram

Note that we included 17 different evaluation methods to assess model performance. Given that each method might encompass multiple variants, we have a total of 30 metrics. A detailed overview of these metrics can be found in Appendix S4.

Table 2: Definitions of six quality dimensions and an overall utility score used in our expert evaluation, along with their corresponding Likert systems.

Evaluation Category	Definition	Likert System
Additions	The impression is not repetitive and does not include unnecessary findings.	3: No additions. 2: Moderate additions. 1: Excessive additions.
Omissions	The impression contains all important findings.	3: No omissions. 2: Moderate omissions. 1: Significant omissions.
Factual correctness	The impression accurately represents the findings and is devoid of factual errors.	3: Correct. 2: Partially correct. 1: Substantially incorrect.
Clarity and organization	The impression is unambiguous, grammatical, and well-organized.	3: Good. 2: Adequate. 1: Poor.
Interpretive and technical jargon	The impression provides appropriate interpretations of the findings and avoids using unnecessary radiologic jargon or details.	3: Appropriate. 2: Partially appropriate. 1: Inappropriate.
Recommendations	The recommendations for patient management, if applicable, are clinically valid.	3: Appropriate. 2: Partially appropriate. 1: Inappropriate.
Overall utility score	Given the impression as an initial draft, consider how many changes would you make to render it suitable for clinical use.	5: Acceptable with no changes needed. 4: Acceptable with minor changes needed. 3: Acceptable with moderate changes needed. 2: Unacceptable with significant changes needed. 1: Unusable.

Results

Benchmarking evaluation metrics

Figure 2 shows the Spearman's ρ correlation between evaluation metrics and quality scores assigned by the first physician (M.S.). BARTScore+PET and PEGASUSScore+PET exhibited the highest correlations with physician judgment ($\rho=0.568$ and 0.563 , $P=0.30$). Therefore, both metrics were employed to determine the top-performing model for expert evaluation. However, their correlation values were still below the degree of inter-reader correlation ($\rho=0.654$). Similar results were observed in the correlation between evaluation metrics and the second physician's scores (Appendix S6). Without adaption to PET reports, the original BARTScore showed lower correlation ($\rho=0.474$, $P<0.001$) compared to BARTScore+PET, but still outperformed traditional evaluation metrics like Recall-Oriented Understudy for Gisting Evaluation-L (ROUGE-L, $\rho=0.398$, $P<0.001$) (31).

The metrics commonly used in radiology report summarization, including ROUGE (31), BERTScore (32) and RadGraph (10), did not demonstrate strong correlation with physician preferences. Additionally, most reference-free metrics, although effective in general text

summarization, showed considerably lower correlation compared to reference-dependent metrics.

Inter-reader correlation	0.654
BARTScore+PET	0.568
PEGASUSScore+PET	0.563
T5Score+PET	0.542
UniEval	0.501
BARTScore	0.474
CHRF	0.433
Moverscore	0.420
BLEU	0.412
BERTScore	0.407
ROUGE-WE-1	0.403
ROUGE-1	0.402
ROUGE-L	0.398
ROUGE-LSUM	0.397
ROUGE-WE-2	0.396
METEOR	0.388
ROUGE-WE-3	0.385
RadGraph	0.384
ROUGE-2	0.379
PRISM	0.369
ROUGE-3	0.345
S ³ -pyr	0.302
S ³ -resp	0.301
Stats-novel trigram	0.292
Stats-density	0.280
CIDEr	0.194
BLANC	0.165
Stats-compression	0.145
SUPERT	0.082
Stats-coverage	0.078
SummaQA	0.075

Figure 2: Spearman’s ρ correlations between different evaluation metrics and quality scores assigned by the first physician. The top row quantifies the inter-reader correlation. Notably, domain-adapted BARTScore (BARTScore+PET) and PEGASUSScore (PEGASUSScore+PET) demonstrate the highest correlations with physician preferences.

Model Performance

Figure 3 illustrates the relative performance of 12 language models assessed using all evaluation metrics considered in this study. For better visualization, metric values have been normalized to [0, 1], with the original values available in Appendix S7. The SOTA encoder-decoder models, including PEGASUS, BART, and T5, demonstrated similar performance across most evaluation metrics. Since BARTScore+PET and PEGASUSScore+PET identified PEGASUS as the top-performing model, we selected it for further expert evaluation.

After being fine-tuned on our PET reports, the medical knowledge enriched models, BioBART (BARTScore+PET: -1.46; ROUGE-L: 38.9) and Clinical-T5 (BARTScore+PET: -1.54; ROUGE-L: 39.4), did not show superior performance compared to their base models, BART (BARTScore+PET: -1.46; ROUGE-L: 38.6) and T5 (BARTScore+PET: -1.52; ROUGE-L: 40.3). Additionally, the four decoder-only models included in this study showed significantly lower performance ($P < 0.001$) compared to the top-tier encoder-decoder LLMs. Interestingly, LLaMA-LoRA (BARTScore+PET: -2.26; ROUGE-L: 27.2) and Alpaca-LoRA (BARTScore+PET: -2.24; ROUGE-L: 28.0), which have been pretrained on one trillion tokens, did not surpass the performance of GPT2 (BARTScore+PET: -2.04, ROUGE-L: 28.7) and OPT (BARTScore+PET: -2.07, ROUGE-L: 28.3).

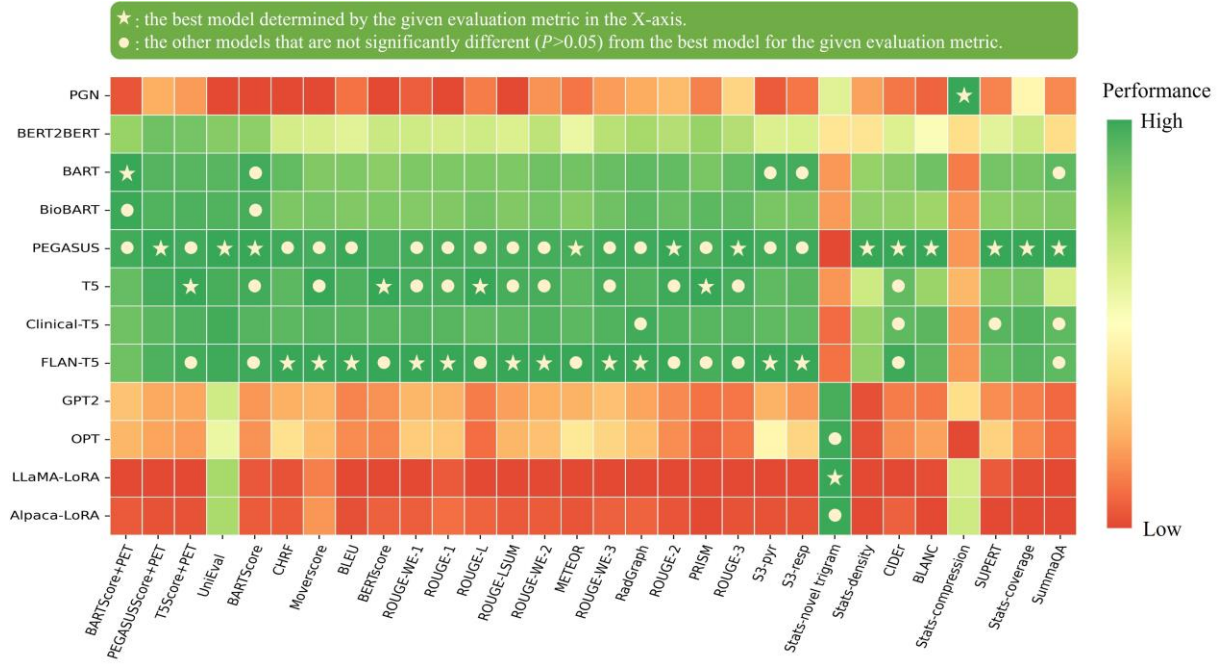


Figure 3: Performance of 12 language models evaluated by the metrics included in this study. The X-axis displays the metrics arranged in descending order of correlation with physician preferences, with higher correlations on the left and lower correlations on the right. For each evaluation metric, values underwent min-max normalization to allow comparison within a single plot. The actual metric values are referenced in Appendix S7. The star denotes the best model for each metric, and the circle denotes the other models that do not have statistically significant difference ($P>0.05$) with the best model.

Expert Evaluation

The distributions of overall utility scores and 6 specific quality scores are illustrated in Figure 4. In total, 83% (60/72) of the PEGASUS-generated impressions were scored as clinically acceptable (scores 3-5), with 60% (43/72) scoring 4 or higher, and 28% (20/72) receiving a score of 5. When the physicians reviewed their own reports, 89% (32/36) of the PEGASUS-generated impressions were clinically acceptable, with a mean utility score of 4.08 (95% CI, 3.72, 4.42). This score was significantly ($P < 0.001$) lower than the mean utility score (4.75, 95% CI, 4.58, 4.89) of the clinical impressions originally dictated by themselves. The discrepancy was primarily attributable to 3 quality dimensions: “factual correctness” (Clinical vs. PEGASUS: 2.97 vs. 2.58, $P=0.001$), “interpretive and technical jargon” (2.94 vs. 2.78, $P=0.034$) and “recommendations” (3.00 vs. 2.69, $P=0.001$).

When the physicians evaluated clinical impressions dictated by other physicians, the mean utility score (4.03, 95% CI, 3.69, 4.33) was significantly lower than scores they assigned to their own impressions ($P < 0.001$), suggesting a strong preference for their individual reporting style. The primary quality dimensions contributing to such difference included “additions” (Physician’s own impressions vs. Other physicians’ impressions: 2.94 vs. 2.75, $P=0.039$) and

“clarity and organization” (2.92 vs. 2.50, $P<0.001$). On average, the physicians considered the overall utility of PEGASUS-generated impressions in their own style to be comparable to the clinical impressions dictated by other physicians (mean utility score: 4.08 vs. 4.03, $P=0.41$).

Figure 5 presents four PEGASUS-generated impressions (findings and background information in Appendix S8) with overall utility scores ranging from 2 to 5. For each case, PEGASUS successfully identified the salient findings, offered interpretations, and provided recommendations. However, the model showed susceptibility to factual incorrectness, including misinterpretation of findings and inconsistent statements of impressions, as evidenced in case 4. Additionally, the model could give overly definite diagnoses, as observed in case 3.

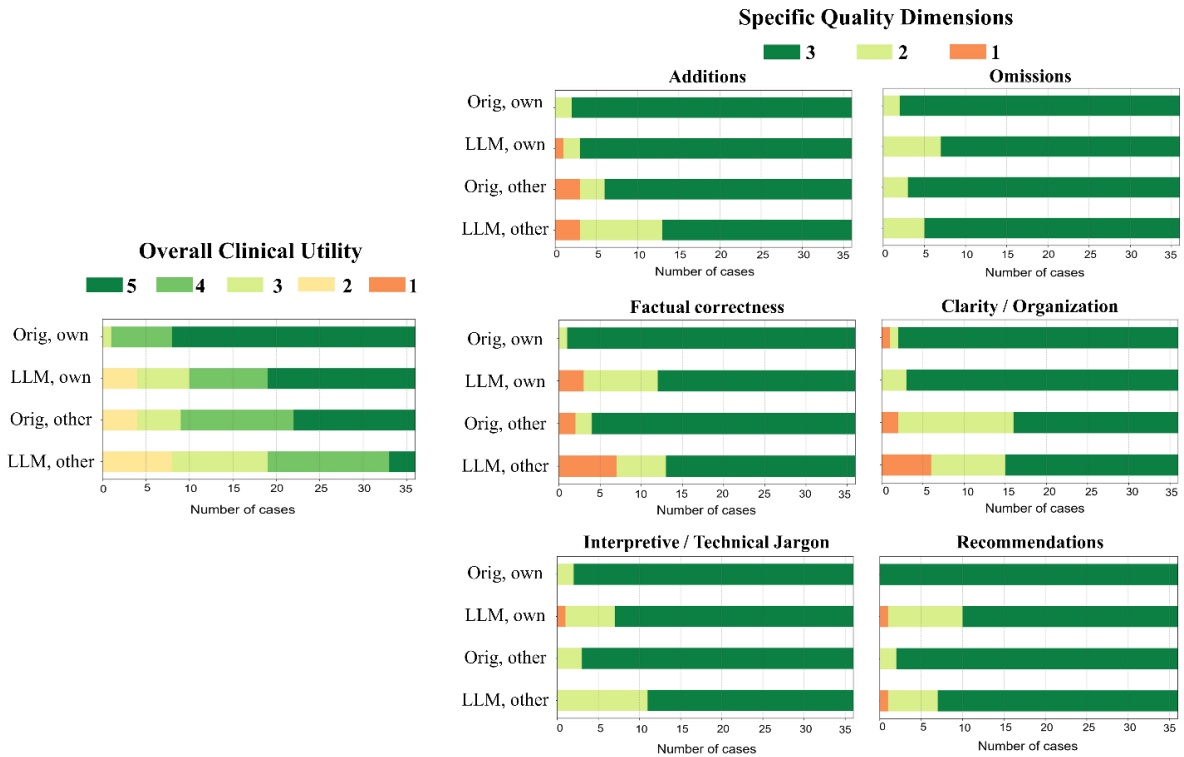


Figure 4: Expert evaluation consisting of an overall utility score and 6 specific quality dimensions. For the physician’s own reports, 89% (32/36) of the PEGASUS-generated impressions were deemed clinically acceptable. The primary reasons for the discrepancy between original clinical impressions and PEGASUS-generated impressions are factual inaccuracies, inappropriate interpretations, and unsuitable recommendations. “Orig, own”: original clinical impressions from the physician’s own reports; “LLM, own”: PEGASUS-generated impressions for the physician’s own reports; “Orig, other”: original clinical impressions from other physicians’ reports; “LLM, other”: PEGASUS-generated impressions for other physicians’ reports.

Deauville Score Prediction

Of the 4,000 test cases, 405 PET lymphoma reports contained DSs in the impression sections. Table 3 presents the DS classification results for all evaluated models. PEGASUS achieved the highest 5-class accuracy (76.7%, 95% CI, 72.0%, 81.0%), while PGN was least effective in deriving DSs. All SOTA encoder-decoder models attained an accuracy exceeding 70%. Among

decoder-only models, GPT2 demonstrated the best performance, with an accuracy of 71.3% (95% CI, 65.8%, 76.4%).

	Original clinical impressions	PEGASUS-generated impressions	Comments on PEGASUS-generated impressions
1	<p>Overall utility score = 5</p> <p>[1] FDG PET/CT demonstrates short-term stability of the solitary nodule within the right upper lobe which has only minimal associated FDG uptake, not elevated above mediastinal blood pool. Given the lack of significant FDG avidity, and the suggestion of macroscopic fat within the nodule on prior diagnostic chest CT, a benign lesion such as a pulmonary hamartoma is a consideration. Could consider short-term follow-up diagnostic CT chest in 3-6 months to assess for interval change.</p> <p>[2] No evidence of suspected FDG avid local nodal mediastinal/hilar or distant metastatic disease.</p> <p>[3] Mildly lobulated nodular soft tissue in the subareolar right breast, without significant FDG avidity. Could correlate with prior mammography, if available. If not, screening mammography is recommended.</p>	<p>Overall utility score = 5</p> <p>[1] FDG PET/CT demonstrates a 1.2 x 1.3 cm subpleural solid nodule within the anteroinferior right upper lobe with mild associated FDG uptake, which is nonspecific by PET criteria for an infectious/inflammatory process versus low-grade primary lung malignancy. Recommend correlation with prior and/or follow-up thoracic CT to assess for interval change in size.</p> <p>[2] No evidence of FDG avid local nodal mediastinal/hilar or distant metastatic disease.</p> <p>[3] Redemonstration of a mildly lobulated nodular area of soft tissue within the subareolar right breast, unchanged compared to [DATE]. This does not appear to have associated hypermetabolic activity.</p>	Good impression by AI
2	<p>Overall utility score = 5</p> <p>[1] FDG PET/CT demonstrates interval resolution of multiple bilateral head/neck, thoracic, and abdominopelvic lymph nodes as well as resolved splenomegaly and intense splenic uptake consistent with complete metabolic response. Deauville 1.</p> <p>[2] No new sites of lymphomatous involvement.</p>	<p>Overall utility score = 4</p> <p>[1] FDG PET/CT demonstrates interval resolution of previously noted hypermetabolic lymphadenopathy in the neck, chest, abdomen, and pelvis consistent with complete metabolic response (Deauville score 1).</p> <p>[2] Decreased homogeneous uptake in the thyroid, right thyroid lobe.</p>	AI impression [2] mentions thyroid uptake which is less important. It does not mention spleen resolution.
3	<p>Overall utility score = 5</p> <p>[1] Slight interval increase in size and FDG uptake of a mildly hypermetabolic subcutaneous soft tissue nodule in the left neck anterior to the sternocleidomastoid muscle which appears more rounded and discrete on the current exam when compared to most recent PET/CT from [DATE]. This finding possibly represents metastatic disease but not particularly avid. Recommend ultrasound-guided sampling for biopsy confirmation.</p> <p>[2] No abnormal FDG uptake to suggest FDG-avid locally recurrent or additional sites of metastatic disease.</p> <p>[3] Probable proteinaceous/hemorrhagic renal cysts. Recommend confirmation with ultrasound.</p>	<p>Overall utility score = 3</p> <p>[1] Slight interval increase in size and FDG uptake of a mildly hypermetabolic subcutaneous soft tissue nodule within the left neck anterior to the sternocleidomastoid muscle at the level of the thyroid cartilage is favored to represent post therapeutic inflammation rather than recurrent disease. Recommend attention on follow-up.</p> <p>[2] No evidence of FDG-avid local or distant metastatic disease.</p>	AI impression [1] is too definitive for benign inflammation when there is still possibility of metastatic disease. It does not mention kidney cysts which is not as important a finding to mention.
4	<p>Overall utility score = 5</p> <p>[1] FDG PET/CT demonstrates intense FDG activity associated with the area of nodular soft tissue thickening at the posterior aspect of the left breast, highly suspicious for recurrent/residual malignancy.</p> <p>[2] Intense FDG avidity associated with the left axillary lymphadenopathy, which is overall unchanged in size and distribution compared to the recent [DATE] CT, also highly suspicious for persistent nodal metastatic disease.</p> <p>[3] No definite evidence of FDG avid osseous metastatic disease. Mild heterogeneous FDG activity, similar to normal bone marrow activity, corresponding to mottled sclerotic and lytic changes in the pelvis, lumbar spine and T8 vertebral body, most likely represents physiologic bone marrow activity at sites of previously treated osseous metastatic disease.</p>	<p>Overall utility score = 2</p> <p>[1] FDG PET/CT demonstrates intense FDG activity associated with the enlarging nodular soft tissue at the posterior aspect of the left breast glandular tissue, which appears to be enlarging on previous CT examinations. This finding is highly suspicious for recurrent malignancy.</p> <p>[2] Moderate-intense FDG avid left axillary lymphadenopathy, similar in size and distribution compared to recent chest CT from [DATE], compatible with nodal metastatic disease.</p> <p>[3] Heterogeneous mild to moderate FDG uptake associated with sclerotic and lytic osseous changes in the pelvis, left clavicle, and T8 vertebral body, with no definite correlative CT bone abnormality on our corresponding low-dose noncontrast CT. These findings are nonspecific but favored to represent posttreatment related inflammatory change rather than residual/recurrent disease. Recommend attention to these sites on follow-up imaging.</p> <p>[4] No evidence of FDG-avid distant metastatic disease in the chest, abdomen, or pelvis.</p>	AI impressions [1] and [2] are well written. However, AI impression [3] assumes inflammatory change when uptake in bone marrow is typically just reactive/physiologic and not inflammatory. Importantly, AI impression [4] is incorrect: there is metastatic disease present as noted in AI impression [2].

Figure 5: A side-by-side comparison of clinical impressions and PEGASUS-generated impressions (overall utility scores range from 2 to 5). The last column presents comments from the physicians in our expert reader study. Sentences with similar semantic meanings in the original clinical impressions and the PEGASUS-generated impressions are highlighted using identical colors. Protected health information (PHI) has been anonymized and denoted with [X], where X may represent age or examination date.

Table 3: Performance of 12 language models on Deauville score prediction

Models	5-Class Accuracy (%)	Weighted Cohen’s κ
PGN	53.5 [46.9, 60.2]	0.528 [0.445, 0.605]
BERT2BERT	69.7 [64.9, 74.3]	0.762 [0.716, 0.805]
BART	75.3 [70.6, 79.7] †	0.806 [0.760, 0.846] †
BioBART	73.9 [69.7, 78.1] †	0.802 [0.761, 0.840] †
PEGASUS	76.7 [72.0, 81.0] *	0.811 [0.767, 0.852] †
T5	76.3 [72.0, 80.6] †	0.814 [0.772, 0.853] *
Clinical-T5	72.5 [67.7, 77.0] †	0.788 [0.745, 0.829] †
FLAN-T5	72.6 [68.0, 77.2] †	0.798 [0.757, 0.837] †
GPT2	71.3 [65.8, 76.4]	0.768 [0.715, 0.817] †
OPT	63.1 [57.7, 68.6]	0.718 [0.665, 0.767]
LLaMA-LoRA	62.9 [56.8, 68.7]	0.708 [0.647, 0.763]
Alpaca-LoRA	70.6 [64.9, 75.8]	0.754 [0.696, 0.805]

Note that data are shown as mean [2.5th percentile, 97.5th percentile]. “*” denotes the best model for each metric, and “†” denotes the other models that have no statistically significant difference ($P > 0.05$) with the best model.

Encoding Physician-specific Styles

Figure 6 shows the PEGASUS-generated impressions given unique identifier tokens associated with two physicians, Physician 1 and Physician 2. Altering a single token in the input could lead to a drastic change in the output impressions. For each case, both impressions managed to capture the salient findings and delivered similar diagnoses, however, their length, level of detail and phrasing generally reflected the respective physician’s style. This reveals the model’s ability to tailor the impressions to individual physicians. The associated findings and background information are presented in Appendix S9.

	Original clinical impression	PEGASUS-generated impression in Physician 1’s style	PEGASUS-generated impression in Physician 2’s style
1	<p>Original clinical impression dictated by Physician 1:</p> <p>[1] FDG PET/CT demonstrates an intensely FDG medial right upper lobe apical pulmonary nodule abutting the pleura, compatible with biopsy-proven primary lung malignancy.</p> <p>[2] Mild to moderate focus of FDG activity in the posterior right lower lobe corresponding to subtle soft tissue pleural thickening at the 8th/9th intercostal region on CT, suspicious for a metastatic pleural implant.</p> <p>[3] No evidence of other sites of FDG avid local nodal or distant metastatic disease.</p> <p>[4] Stable non-FDG left adrenal gland nodule dating to [DATE], most consistent with a benign myelipoma..</p>	<p>[1] FDG PET/CT demonstrates an intensely FDG avid 1.5 x 1.6 cm right upper lobe apical segment pulmonary nodule, consistent with biopsy-proven primary lung malignancy.</p> <p>[2] Mild to moderate FDG activity corresponding right lower lobe posterior pleural thickening at the 8th/9th intercostal region, suspicious for a pleural metastatic implant.</p> <p>[3] No evidence of other sites of suspected PET avid local nodal or distant metastatic disease</p> <p>[4] Non-FDG avid 1.3 cm left adrenal nodule, with fat attenuation on noncontrast CT, which is indeterminate. Recommend adrenal protocol CT or MRI for further evaluation.</p>	<p>[1] Right upper lobe primary lung malignancy with suspected right lower lobe pleural metastasis.</p> <p>[2] No evidence of nodal or distant metastases.</p> <p>[3] Indeterminate left adrenal nodule can be followed on future surveillance imaging.</p>
2	<p>Original clinical impression dictated by Physician 2:</p> <p>Primary right upper lobe lung malignancy without evidence for nodal or distant metastases.</p>	<p>[1] FDG PET/CT demonstrates an intensely FDG avid right upper lobe mass consistent with biopsy-proven primary lung malignancy.</p> <p>[2] No evidence of other sites of abnormal FDG uptake to suggest locoregional or distant metastatic disease.</p>	<p>Right upper lobe primary lung malignancy without evidence of nodal or distant metastases.</p>

Figure 6: Examples of PEGASUS-generated impressions customized for the physician’s reporting style. The first column shows the original clinical impressions: the first example from Physician 1 and the second from Physician 2. Subsequent columns present impressions generated in the style of Physician 1 and Physician 2, respectively. For each case, both impressions capture the critical findings and deliver similar diagnosis. However, their length, level of detail and phrasing generally reflect each physician’s unique style. Sentences with similar semantic meanings in the original clinical impressions and the PEGASUS-generated impressions are highlighted using identical colors.

Discussion

In this work, we trained 12 language models on the task of PET impression generation. To identify the best metrics to evaluate model-generated impressions, we benchmarked 30 evaluation metrics against quality scores assigned by physicians and found that domain-adapted text-generation-based metrics, namely BARTScore+PET and PEGASUSScore+PET, exhibited the strongest correlation with physician preferences. These metrics selected PEGASUS as the top-performing LLM for our expert evaluation. A total of 72 cases were reviewed by three NM physicians, and the large majority of PEGASUS-generated impressions were rated as clinically acceptable. Leveraging a specific token in the input to encode the reading physician’s identity, we enabled LLMs to learn different reporting styles and generate personalized impressions. When physicians assessed impressions generated in their own style, they considered these impressions to be of comparable overall utility to the impressions dictated by other physicians. Given the average inference time of 1.6 s per case, our PEGASUS model has the potential to be

integrated into clinical workflows and accelerate the drafting of PET impressions. It could also lead to more consistent, and potentially more standardized, PET reporting considering the model’s ability to adapt impressions to a specific style.

Past research on text summarization has introduced numerous evaluation metrics for assessing the quality of AI-generated summaries. However, when these metrics were employed to evaluate PET impressions, the majority did not align closely with physician judgements. This observation is consistent with findings from other works that evaluated medical document (33) or clinical note summarization (12). The avenue to improvement could be training the model-based metric (34) using expert-annotated data.

Based on our comparison of 12 language models, we observed that the biomedical-domain pretrained LLMs did not outperform their base models. This could be attributed to two reasons. First, our large training set diminished the benefits of medical-domain adaptation. Second, the corpora, such as MIMIC-III and PubMed, likely had limited PET relevant content, making pretraining less effective for our task. Additionally, we found that the large decoder-only models showed inferior performance in summarizing PET findings compared to the SOTA encoder-decoder models. It stems from their lack of an encoder mechanism that can efficiently distill the essence of input sequences. In this study, we did not test large proprietary models like GPT4 due to data ownership issues and the inability to fine-tune the models for personalized impressions. Recent works (7, 8) explored their capability in radiology report summarization using the in-context learning technique. The question of whether this approach could surpass the full fine-tuning method for public LLMs and its suitability for clinical use remains to be answered.

While most PEGASUS-generated impressions were deemed clinically acceptable in expert evaluation, it is crucial to understand what mistakes are commonly committed by the LLM. First, the main problem in model-generated impressions is factual inaccuracies, which manifest as misinterpretation of findings or contradictory statements of impressions. Second, the diagnoses given by the LLM could sometimes be overly definite without adequate supporting evidence. Third, some recommendations for clinical follow-up are non-specific, offering limited guidance for patient management. It is worth mentioning that final diagnoses and recommendations are usually not included in the report findings and must be inferred by the model. These observations underscore the need for review and appropriate editing by physicians before report finalization. Of note, LLM-based impression generation can be akin to preliminary impression drafts by radiology resident trainees provided for review by the radiology faculty in an academic training setting.

This study had several limitations. First, when fine-tuning LLaMA and Alpaca, we only investigated a lightweight domain adaptation method, LoRA, constrained by computational resources. Second, we controlled the style of generated impressions by altering a specific token in the input, leaving other potential techniques unexplored. Lastly, our training dataset was restricted to a single institution. Future work should be expanding our research to a multi-center study.

In conclusion, we show that LLMs have the potential to produce personalized and clinically-useful PET impressions. LLMs could expedite PET reporting by automatically drafting initial impressions based on the findings.

References

1. Niederkoher RD, Greenspan BS, Prior JO, et al. Reporting Guidance for Oncologic 18 F-FDG PET/CT Imaging. *J Nucl Med*. 2013;54(5):756–761. doi: 10.2967/jnumed.112.112177.
2. Hartung MP, Bickle IC, Gaillard F, Kanne JP. How to Create a Great Radiology Report. *RadioGraphics*. 2020;40(6):1658–1670. doi: 10.1148/rg.2020200020.
3. Zhang Y, Ding DY, Qian T, Manning CD, Langlotz CP. Learning to Summarize Radiology Findings. *arXiv*; 2018. <http://arxiv.org/abs/1809.04698>. Accessed March 1, 2023.
4. Hu J, Li Z, Chen Z, Li Z, Wan X, Chang T-H. Graph Enhanced Contrastive Learning for Radiology Findings Summarization. *arXiv*; 2022. <http://arxiv.org/abs/2204.00203>. Accessed March 2, 2023.
5. Delbrouck J-B, Varma M, Langlotz CP. Toward expanding the scope of radiology report summarization to multiple anatomies and modalities. *arXiv*; 2022. <http://arxiv.org/abs/2211.08584>. Accessed March 2, 2023.
6. Liu Z, Zhong A, Li Y, et al. Radiology-GPT: A Large Language Model for Radiology. *arXiv*; 2023. <http://arxiv.org/abs/2306.08666>. Accessed July 20, 2023.
7. Sun Z, Ong H, Kennedy P, et al. Evaluating GPT4 on Impressions Generation in Radiology Reports. *Radiology*. 2023;307(5):e231259. doi: 10.1148/radiol.231259.
8. Ma C, Wu Z, Wang J, et al. ImpressionGPT: An Iterative Optimizing Framework for Radiology Report Summarization with ChatGPT. *arXiv*; 2023. <http://arxiv.org/abs/2304.08448>. Accessed August 14, 2023.
9. Johnson AEW, Pollard TJ, Berkowitz SJ, et al. MIMIC-CXR, a de-identified publicly available database of chest radiographs with free-text reports. *Sci Data*. 2019;6(1):317. doi: 10.1038/s41597-019-0322-0.
10. Hu J, Li J, Chen Z, et al. Word Graph Guided Summarization for Radiology Findings. *arXiv*; 2021. <http://arxiv.org/abs/2112.09925>. Accessed August 22, 2023.
11. Smit A, Jain S, Rajpurkar P, Pareek A, Ng AY, Lungren MP. CheXbert: Combining Automatic Labelers and Expert Annotations for Accurate Radiology Report Labeling Using BERT. *arXiv*; 2020. <http://arxiv.org/abs/2004.09167>. Accessed August 27, 2023.

12. Abacha AB, Yim W, Michalopoulos G, Lin T. An Investigation of Evaluation Metrics for Automated Medical Note Generation. arXiv; 2023. <http://arxiv.org/abs/2305.17364>. Accessed August 27, 2023.
13. Kayaalp M, Browne AC, Dodd ZA, Sagan P, McDonald CJ. De-identification of Address, Date, and Alphanumeric Identifiers in Narrative Clinical Reports. AMIA Annu Symp Proc; 2014; 2014: 767–776. PMID: 25954383; PMCID: PMC4419982.
14. Castellino SM, Pei Q, Parsons SK, et al. Brentuximab Vedotin with Chemotherapy in Pediatric High-Risk Hodgkin’s Lymphoma. N Engl J Med. 2022;387(18):1649–1660. doi: 10.1056/NEJMoa2206660.
15. Wang Y, Kordi Y, Mishra S, et al. Self-Instruct: Aligning Language Models with Self-Generated Instructions. arXiv; 2023. <http://arxiv.org/abs/2212.10560>. Accessed June 20, 2023.
16. Rohan T, Ishaan G, Tianyi Z, et al. Stanford Alpaca: An Instruction-following LLaMA model. GitHub; 2023. https://github.com/tatsu-lab/stanford_alpaca. Accessed June 20, 2023.
17. Lewis M, Liu Y, Goyal N, et al. BART: Denoising Sequence-to-Sequence Pre-training for Natural Language Generation, Translation, and Comprehension. arXiv; 2019. <http://arxiv.org/abs/1910.13461>. Accessed March 7, 2023.
18. Zhang J, Zhao Y, Saleh M, Liu PJ. PEGASUS: Pre-training with Extracted Gap-sentences for Abstractive Summarization. arXiv; 2020. <http://arxiv.org/abs/1912.08777>. Accessed March 7, 2023.
19. Raffel C, Shazeer N, Roberts A, et al. Exploring the Limits of Transfer Learning with a Unified Text-to-Text Transformer. arXiv; 2020. <http://arxiv.org/abs/1910.10683>. Accessed June 20, 2023.
20. Wei J, Bosma M, Zhao VY, et al. Finetuned Language Models Are Zero-Shot Learners. arXiv; 2022. <http://arxiv.org/abs/2109.01652>. Accessed August 15, 2023.
21. Yuan H, Yuan Z, Gan R, Zhang J, Xie Y, Yu S. BioBART: Pretraining and Evaluation of A Biomedical Generative Language Model. arXiv; 2022. <http://arxiv.org/abs/2204.03905>. Accessed August 15, 2023.
22. Lu Q, Dou D, Nguyen TH. ClinicalT5: A Generative Language Model for Clinical Text. Findings of the Association for Computational Linguistics: EMNLP 2022, pages 5436–5443, Abu Dhabi, United Arab Emirates. Association for Computational Linguistics. doi: 10.18653/v1/2022.findings-emnlp.398.
23. Chen C, Yin Y, Shang L, et al. bert2BERT: Towards Reusable Pretrained Language Models. Proceedings of the 60th Annual Meeting of the Association for Computational Linguistics (Volume 1: Long Papers). Dublin, Ireland: Association for Computational Linguistics; 2022. p. 2134–2148. doi: 10.18653/v1/2022.acl-long.151.
24. Ziegler DM, Stiennon N, Wu J, et al. Fine-Tuning Language Models from Human Preferences. arXiv; 2020. <http://arxiv.org/abs/1909.08593>. Accessed June 20, 2023.
25. Zhang S, Roller S, Goyal N, et al. OPT: Open Pre-trained Transformer Language Models. arXiv; 2022. <http://arxiv.org/abs/2205.01068>. Accessed August 15, 2023.
26. Touvron H, Lavril T, Izacard G, et al. LLaMA: Open and Efficient Foundation Language Models. arXiv; 2023. <http://arxiv.org/abs/2302.13971>. Accessed August 14, 2023.

27. Hu EJ, Shen Y, Wallis P, et al. LoRA: Low-Rank Adaptation of Large Language Models. arXiv; 2021. <http://arxiv.org/abs/2106.09685>. Accessed August 15, 2023.
28. Yuan W, Neubig G, Liu P. BARTScore: Evaluating Generated Text as Text Generation. arXiv; 2021. <http://arxiv.org/abs/2106.11520>. Accessed August 15, 2023.
29. Huemann Z, Lee C, Hu J, Cho SY, Bradshaw T. Domain-adapted large language models for classifying nuclear medicine reports. arXiv; 2023. <http://arxiv.org/abs/2303.01258>. Accessed March 17, 2023.
30. Smith L, Tanabe LK, Ando RJ, et al. Overview of BioCreative II gene mention recognition. *Genome Biol.* 2008;9(S2):S2. doi: 10.1186/gb-2008-9-s2-s2.
31. Lin CY. ROUGE: A package for automatic evaluation of summaries. In *Text Summarization Branches Out*, Barcelona, Spain, July 2004. Association for Computational Linguistics, 2004; 74–81. <https://aclanthology.org/W04-1013/>.
32. Zhang T, Kishore V, Wu F, Weinberger KQ, Artzi Y. BERTScore: Evaluating Text Generation with BERT. arXiv; 2020. <http://arxiv.org/abs/1904.09675>. Accessed August 22, 2023.
33. Wang LL, Otmakhova Y, DeYoung J, et al. Automated Metrics for Medical Multi-Document Summarization Disagree with Human Evaluations. arXiv; 2023. <http://arxiv.org/abs/2305.13693>. Accessed August 22, 2023.
34. Clark E, Rijhwani S, Gehrmann S, et al. SEAHORSE: A Multilingual, Multifaceted Dataset for Summarization Evaluation. arXiv; 2023. <http://arxiv.org/abs/2305.13194>. Accessed August 22, 2023.

Supplementary Materials

Materials and Methods

Appendix S1: Statistics of PET Reports

Among 37,370 retrospective PET reports in our internal dataset, 92.7% (34,655/37,370) pertained to PET/CT whole-body (including skull base to thigh and skull vertex to feet) scans, 1.7% (649/37,370) to PET/MRI whole-body (including skull base to thigh and skull vertex to feet) scans, 5.5% (2,066/37,370) to PET limited area (including brain, cardiac and myocardial) scans. The findings section in a PET report had 346 [249, 472] (median [25th percentile, 75th percentile]) words, and the impression section had 86 [53, 130] words.

Appendix S2: “Description” and “Radiologist” Fields

In the input template, “Description” denotes the categories of PET scans, with their counts provided in Figure E1 (a). “Radiologist” accommodates a single token that encodes the reading physician’s identity. The list of these tokens as well as their counts are given in Figure E1 (b). Notably, only physicians who dictated more than 100 PET reports are included.

Description	Counts	Tokens associated with dictating physicians	Counts	Tokens associated with dictating physicians	Counts	Tokens associated with dictating physicians	Counts
PET CT WHOLE BODY	34,655	James	7184	Charles	827	Andrew	275
PET CT BRAIN	1,424	Robert	4872	Christopher	677	Kenneth	258
PET MRI WHOLE BODY	649	John	4827	Daniel	507	Kevin	241
PET CT MYOCARDIAL	407	Michael	4484	Matthew	460	Brian	178
PET MRI BRAIN	100	David	3096	Anthony	408	George	173
PET CT LIMITED AREA	91	William	2492	Mark	400	Timothy	157
PET MRI LIMITED AREA	29	Richard	1828	Donald	370	Ronald	156
PET CT CARDIAC	15	Joseph	1231	Steven	358	Edward	154
		Thomas	835	Paul	351	Jason	103

(a) (b)

Figure E1: (a) shows the descriptions of examination categories in our internal dataset. (b) lists the reading physicians’ unique identifier tokens.

Appendix S3: Models for PET Report Summarization

1. **PGN** (1) It is an encoder-decoder model built on the bidirectional long short-term memory (LSTM) architecture. The decoder can choose between copying a word directly from the input or generating a new one from the vocabulary. The model was modified to accommodate both background information and findings, as suggested in (1). We adapted the original implementation (available at github.com/yuhaozhang/summarize-radiology-findings) to fit our task and made the model weights accessible on GitHub: github.com/xtie97/PET-PGN.

2. **BERT2BERT** (2): It is an encoder-decoder model built on the transformer architecture. We utilized Clinical-Longformer (3) as the encoder and RoBERTa (4) as the decoder. The weights of the cross-attention layers were randomly initialized. Pretrained Clinical-Longformer is available on Hugging Face: huggingface.co/yikuan8/Clinical-Longformer and pretrained RoBERTa is available at huggingface.co/roberta-base.

3. **BART** (5): It is an encoder-decoder model built on the transformer architecture. BART introduced a denoising auto-encoder for pretraining, involving reconstructing the original texts from the corrupted samples. Pretrained BART is available at huggingface.co/facebook/bart-large.

4. **BioBART** (6): The model shares the same architecture with BART (5) but underwent further training on the PubMed dataset. Pretrained BioBART is available at huggingface.co/GanjinZero/biobart-large.
5. **PEGASUS** (7): It is an encoder-decoder model built on the transformer architecture. PEGASUS introduced a novel pretraining objective (gap sentence prediction), involving masking important sentences from documents and forcing the model to recover them based on the remaining sentences. Pretrained PEGASUS is available at huggingface.co/google/pegasus-large.
6. **T5** (8): It is an encoder-decoder model built on the transformer architecture. T5 established a unified framework that treats almost all natural language tasks as a text-to-text problem. Instead of the original T5, we used T5v1.1 that had multiple modifications of the architecture and was solely pretrained on unsupervised tasks. The model weights are available at huggingface.co/google/t5-v1.1-large.
7. **Clinical-T5** (9): It is tailored to handle the language structures, terminologies in medical documents by further pretraining T5 on the MIMIC-III dataset (10). The model weights are available at huggingface.co/luqh/ClinicalT5-large.
8. **Flan-T5** (11): It is a variant of T5 that underwent instruction finetuning in a mixture of tasks. This enabled Flan-T5 to achieve enhanced performance compared to the original T5 in various downstream applications. The model weights are available at huggingface.co/google/flan-t5-large.
9. **GPT2** (12): It is a decoder-only model built on the transformer architecture. Unlike the encoder-decoder models, GPT2 is pretrained on a massive corpus of text to predict the next word in a sequence. The model weights are available at huggingface.co/gpt2-xl.
10. **OPT** (13): It is a series of open-sourced, decoder-only transformers with varying sizes from 125M to 175B. The pretrained weights are available at huggingface.co/facebook/opt-1.3b.
11. **LLaMA-LoRA**: LLaMA (14) is a collection of decoder-only transformers, ranging from 7B to 65B. LLaMA-13B showed superior performance compared to GPT3 on most benchmarks. In this study, we chose LLaMA-7B and used LoRA (15) to accelerate training and reduce memory usage. The hyperparameters of the LoRA module are listed as follows: the rank of the low-rank factorization is 8, the scaling factor for the rank is 16, the dropout rate is 0.05, the target modules for LoRA are projection layers in query (q_proj) and value (v_proj). The model weights for LLaMA are available upon request.
12. **Alpaca-LoRA**: Alpaca (16) is the instruction tuned LLaMA-7B model that behaves qualitatively similarly to some closed-source large language models (LLMs), including OpenAI’s text-davinci-003. When we finetuned Alpaca, we retained the same hyperparameters as used in LLaMA-LoRA. The weight difference between LLaMA and Alpaca is available at huggingface.co/tatsu-lab/alpaca-7b-wdiff.

All twelve language models were trained using the standard teacher-forcing algorithm. The training objective can be written as a maximum likelihood problem:

$$\theta^* = \operatorname{argmax}_{\theta} \sum_t \sum_i \log p_{G(\theta)}(r_t^{(i)} | S^{(i)}, R_{<t}^{(i)}; \theta)$$

Where θ denotes the parameters of model G , $p_{G(\theta)}$ estimates the probability of the next word r_t given the previous sequence $R_{<t}$ in the reference text and the source text S . Superscript t denotes the word position in the reference text and i denotes a single sample. The AdamW optimizer (17) was employed to optimize this log-likelihood loss. The learning rates for the transformer-based LLMs were selected from $\{5e-5, 1e-4, 2e-4, 4e-4\}$ based on the Recall-Oriented Understudy for Gisting Evaluation-L (ROUGE-L) (18) in the validation set. We adopted the beam search decoding algorithm to generate impressions, setting the number of beams to 4. Additionally, we blocked the repeated trigram in the generated text and applied a length penalty of 2. For PGN, we followed the training and inference

parameters specified in the original paper (1). Table E1 summarizes the settings for each model in this study.

The learning environment requires at least 2 NVIDIA A100 GPUs and the following Python (3.8.8) libraries: PyTorch (1.13.1), transformer (4.30.0), fastAI (2.7.11), deepspeed (0.9.2). Except for LLaMA-LoRA and Alpaca-LoRA, all models were trained on a single NVIDIA A100 GPU, with each epoch taking 50-120 minutes. LLaMA-LoRA and Alpaca-LoRA, however, required two NVIDIA A100 GPUs and took 4.5 hours per epoch.

Table E1: Training and inference settings of language models investigated in this study.

Language models	Finetuning methods	Number of trainable parameters	Learning rate	Total batch size	Number of training epochs	Number of beams for beam search
PGN	Full finetuning	8.3 M	1e-3 *	25 *	30 *	5 *
BERT2BERT	Full finetuning	301.7 M	1e-4	32	15	4
BART	Full finetuning	406.3 M	5e-5	32	15	4
BioBART	Full finetuning	406.3 M	5e-5	32	15	4
PEGASUS	Full finetuning	568.7 M	2e-4	32	15	4
T5	Full finetuning	783.2 M	4e-4	32	15	4
Clinical-T5	Full finetuning	737.7 M	4e-4	32	15	4
Flan-T5	Full finetuning	783.2 M	4e-4	32	15	4
GPT2	Full finetuning	1.5 B	5e-5	32	15	4
OPT	Full finetuning	1.3 B	1e-4	32	15	4
LLaMA-LoRA	LoRA	4.2 M	2e-4	128	20	4
Alpaca-LoRA	LoRA	4.2 M	2e-4	128	20	4

Note that “*” denotes the hyperparameters directly taken from the original paper. Total batch size = training batch size per device \times number of GPU devices \times gradient accumulation steps.

Appendix S4: Benchmarking Evaluation Metrics

Both nuclear medicine (NM) physicians scored the quality of model-generated impressions on a 5-point Likert scale. The definition of each level are given in Table E2.

Table E2: Definition of the 5-point Likert scale for evaluating the quality of model-generated impressions.

Score	Definition
5	Clinically acceptable impressions. The generated impression is consistent with the key clinical findings and align with the physician’s impression. Well organized and readable.
4	Nearly acceptable impressions. The generated impression is mostly consistent with the key clinical findings and aligns overall with the physician’s impression. Minor additions or subtractions. Organized and readable.
3	Moderately acceptable impressions. The generated impression has some inconsistencies with the key clinical findings and mostly aligns with the physician’s impression. Moderate additions or subtractions.
2	Unacceptable impressions. The generated impression is factually incorrect in parts and/or missing some key clinical findings and may not completely align with the physician’s impression. Major additions or subtractions.
1	Unusable impressions. The generated impression is factually incorrect and/or misses most of the key clinically findings and does not align with the physician’s impression.

We investigated a broad spectrum of evaluation metrics, comprising 17 different methods.

1. **ROUGE** (18): It measures the number of overlapping textual units between generated and reference texts. ROUGE-N (N=1,2,3) measures the overlap of N-grams, and ROUGE-L measures the overlap of longest common subsequence. ROUGE-LSUM extends ROUGE-L by computing the ROUGE-L for each sentence, and then summing them up.
2. **BLEU** (19): It computes the precision of n-gram overlap (n ranges from 1 to 4) between generated and reference texts with a brevity penalty.
3. **CHRF** (20): It computes the character-based n-gram overlap between the output sequence and the reference sequence. In this study, we set the n-gram length to 10.
4. **METEOR** (21): It computes an alignment of the generated text and the reference text based on synonymy, stemming, and exact word matching.
5. **CIDEr** (22): It computes the term frequency-inverse document frequency (TF-IDF) vectors for both human and machine-generated texts based on the n-gram (n ranges from 1 to 4) co-occurrence, and then measures the cosine similarity of the two vectors.
6. **ROUGE-WE** (23): It is an extension of the ROUGE metric, designed to assess the semantic similarity between generated and reference texts using pretrained word embeddings.
7. **BERTScore** (24): It evaluates the cosine similarity of contextual embeddings from BERT for each token in the output and reference sequences.
8. **MoverScore** (25): Similar to BERTScore, it leverages the power of BERT’s contextual embeddings to measure the semantic similarity between generated and reference texts. Instead of token-level cosine similarity, MoverScore calculates the Earth Mover’s Distance between the embeddings of the two texts.
9. **RadGraph** (26): It is a specialized evaluation metric tailored for radiology report summarization. RadGraph works by initially extracting clinical entities and their relations from the model-generated impression and the original clinical impression. Leveraging this data, it constructs knowledge graphs to compare the content coverage and structural coherence between the two impressions.

10. **BARTScore** (27): It leverages a pretrained BART model to compute the log probability of generating one text conditioned on another text. In this study, BARTScore is the BART model finetuned on the CNN Daily Mail dataset. BARTScore+PET is the BART model finetuned on our internal PET report dataset. PEGASUSScore+PET is the PEGASUS model finetuned on our internal dataset. T5Score+PET is the Flan-T5 model finetuned on our internal dataset. The training settings are the same as those in Table E1, except for different training/validation splits and random seeds.

11. **PRISM** (28): It is an evaluation metric used in multilingual machine translation. PRISM employs a sequence-to-sequence model to score the machine-generated output conditioned on the human reference.

12. **S³** (29): It uses previously proposed evaluation metrics, including ROUGE and ROUGE-WE, as input features for a regression model to estimate the quality score of the generate text. S³-resp is based on a model trained with human annotations following the responsiveness scheme, while S³-pyr follows the pyramid scheme.

13. **UniEval** (30): It first constructs pseudo summaries by perturbing reference summaries, then defines evaluation dimensions using different prompt templates. The model is trained to differentiate pseudo data from reference data in a Boolean question-answering framework. While UniEval evaluates coherence, consistency, fluency, and relevance, we only present the overall score which is the average of these 4 dimensions.

14. **SummaQA** (31): It creates questions from the source document by masking entities. The generated text is then evaluated by a question-answering BERT model, with results reported in terms of the F1 overlap score.

15. **BLANC** (32): It measures how well a generated summary can help improve the performance of a pretrained BERT model in understanding each sentence from the source document with masked tokens.

16. **SUPERT** (33): It creates pseudo-reference summaries by extracting important sentences from the source document and then measures the semantic similarity between the generated text and this pseudo reference.

17. **Stats (Data Statistics)** (34): Stats-compression refers to the word ratio of the source document to its summary. Stats-coverage measures the proportion of words in the generated text that also appear in the source document. Stats-density is the average length of the fragment (e.g., sentence in the source document) from which each summary word is extracted. Stats-novel trigram is the percentage of trigrams present in the summary but absent in the source document.

For the metrics that have precision, recall and F1, we only present the F1 score, which is the harmonic mean of precision and recall. The evaluation codes are partially adapted from (35) and made available on GitHub: github.com/xtie97/PET-Report-Summarization/tree/main/evaluation_metrics.

Appendix S5: Implementation Details of Additional Analysis

1. **Deauville score (DS) extraction**: Whole-body PET reports that contained physician assigned DSs in the impression sections were identified by searching for the term “Deauville” and its common misspellings. N-gram analysis was then performed to extract the score for each case. Among 405 cases with DSs in the impression section, 34 cases also had DSs in the findings section. To avoid leakage, we removed the scores in these findings. If multiple DSs were present in the impression, the highest value was used to represent the exam-level DS (36). It is likely that model-generated impressions did not contain DSs in some cases, but their original clinical impressions had DSs or vice versa. Considering that we did not force the model to generate DSs in the impressions, we excluded these cases when calculating 5-class accuracy and Cohen’s κ index. Except for PGN, all language models had at least 250 cases available for evaluating the performance of DS prediction.

2. Controlling reporting styles in output impressions: To alter the style, we directly change the reading physician’s identifier token to any option in Figure E1 (b). In this study, "Physician 1" corresponds to "Robert," "Physician 2" to "William," and "Physician 3" to "James". To illustrate, if we aim to generate the impression for a whole-body PET/CT report in the style of Physician 1, we need to replace the original reading physician’s token with the token associated with Physician 1 (i.e., “Robert”). For encoder-decoder models, the input should start with “Description: PET CT WHOLE BODY Radiologist: Robert”. For decoder-only models, the instruction should be “Instruction: Derive the impression from the given PET CT WHOLE BODY report for Robert”.

Results

Appendix S6: Correlation of Evaluation Metrics with the Second Physician’s Scores

Figure E2 presents the Spearman’s ρ correlation between evaluation metrics and quality scores assigned by the second physician (S.Y.C.). BARTScore+PET and PEGASUSScore+PET showed the highest correlation values. Both physicians agreed upon the top-5 metrics most correlated with physician preferences, namely BARTScore+PET, PEGASUSScore+PET, T5Score+PET, UniEval and BARTScore.

Inter-reader correlation					
0.654					
BARTScore+PET	0.564	METEOR	0.421	ROUGE-3	0.368
PEGASUSScore+PET	0.550	BLEU	0.418	RadGraph	0.346
UniEval	0.536	S ³ -resp	0.418	Stats-density	0.305
BARTScore	0.533	ROUGE-L	0.412	CIDEr	0.302
T5Score+PET	0.508	ROUGE-2	0.386	Stats-novel trigram	0.270
BERTScore	0.453	ROUGE-WE-1	0.385	BLANC	0.199
Moverscore	0.438	ROUGE-WE-2	0.384	SUPERT	0.195
PRISM	0.430	ROUGE-1	0.372	Stats-coverage	0.147
S ³ -pyr	0.424	ROUGE-LSUM	0.368	Stats-compression	0.069
CHRF	0.421	ROUGE-WF-3	0.368	SummaQA	0.015

Figure E2: Spearman’s ρ correlations between different evaluation metrics and quality scores assigned by the second physician.

Appendix S7: Model Performance

Figure E3 presents the performance evaluation of 12 language models across all 30 metrics (17 different methods) considered in this study. All numbers in this figure are actual metric values. In the first column, we sort the metrics in descending order of correlation with the first physician’s (M.S.) preference.

	PGN	BERT2 BERT	BART	BioBART	PEGASUS	T5	Clinical-T5	FLAN-T5	GPT2	OPT	LLaMA- LoRA	Alpaca-LoRA
BARTScore +PET	-2.25 [-2.26, -2.23]	-1.61 [-1.63, -1.60]	-1.46 * [-1.47, -1.44]	-1.46 † [-1.47, -1.45]	-1.47 † [-1.48, -1.46]	-1.53 [-1.54, -1.51]	-1.54 [-1.56, -1.53]	-1.54 [-1.56, -1.53]	-2.04 [-2.05, -2.03]	-2.07 [-2.08, -2.05]	-2.27 [-2.28, -2.25]	-2.24 [-2.25, -2.22]
PEGASUSScore +PET	-2.25 [-2.27, -2.23]	-1.55 [-1.56, -1.53]	-1.49 [-1.50, -1.47]	-1.48 [-1.49, -1.47]	-1.44 * [-1.45, -1.42]	-1.46 [-1.47, -1.45]	-1.50 [-1.51, -1.48]	-1.48 [-1.49, -1.46]	-2.26 [-2.28, -2.24]	-2.27 [-2.28, -2.25]	-2.48 [-2.50, -2.46]	-2.46 [-2.47, -2.44]
TSScore+PET	-2.20 [-2.22, -2.19]	-1.52 [-1.53, -1.50]	-1.46 [-1.47, -1.44]	-1.44 [-1.46, -1.43]	-1.42 † [-1.43, -1.40]	-1.41 * [-1.42, -1.39]	-1.45 [-1.46, -1.43]	-1.42 † [-1.44, -1.41]	-2.17 [-2.19, -2.16]	-2.20 [-2.21, -2.18]	-2.38 [-2.40, -2.36]	-2.36 [-2.38, -2.34]
UniEval	0.34 [0.34, 0.35]	0.72 [0.71, 0.72]	0.76 [0.75, 0.76]	0.76 [0.76, 0.77]	0.78 * [0.78, 0.78]	0.77 [0.77, 0.78]	0.77 [0.77, 0.77]	0.78 [0.77, 0.78]	0.64 [0.63, 0.64]	0.59 [0.59, 0.60]	0.68 [0.68, 0.69]	0.68 [0.67, 0.68]
BARTScore	-3.97 [-3.99, -3.95]	-3.20 [-3.22, -3.18]	-3.06 † [-3.08, -3.04]	-3.07 † [-3.09, -3.05]	-3.05 * [-3.07, -3.03]	-3.07 † [-3.09, -3.05]	-3.10 [-3.12, -3.08]	-3.06 † [-3.08, -3.04]	-3.81 [-3.83, -3.80]	-3.82 [-3.83, -3.80]	-3.93 [-3.95, -3.92]	-3.93 [-3.94, -3.91]
CHRF	25.3 [24.9, 25.6]	36.3 [35.9, 36.7]	40.9 [40.5, 41.3]	40.0 [39.6, 40.4]	42.0 † [41.6, 42.4]	41.1 [40.7, 41.5]	41.1 [40.7, 41.5]	42.2 * [41.8, 42.6]	29.2 [28.9, 29.6]	31.6 [31.3, 31.9]	25.7 [25.4, 26.0]	26.0 [25.7, 26.3]
Moverscore	0.565 [0.563, 0.568]	0.592 [0.590, 0.594]	0.601 [0.599, 0.603]	0.602 [0.600, 0.604]	0.607 † [0.605, 0.608]	0.607 † [0.605, 0.608]	0.605 [0.604, 0.607]	0.607 † [0.606, 0.609]	0.575 [0.574, 0.576]	0.576 [0.575, 0.577]	0.570 [0.569, 0.570]	0.572 [0.571, 0.573]
BLEU	10.8 [10.5, 11.1]	18.7 [18.3, 19.1]	22.6 [22.2, 23.1]	22.5 [22.1, 22.9]	24.7 † [24.2, 25.1]	24.1 [23.7, 24.6]	23.9 [23.5, 24.4]	24.7 * [24.3, 25.2]	11.4 [11.1, 11.6]	11.7 [11.4, 11.9]	9.3 [9.1, 9.6]	9.6 [9.4, 9.9]
BERTScore	0.673 [0.735, 0.739]	0.723 [0.735, 0.739]	0.735 [0.735, 0.739]	0.737 [0.735, 0.739]	0.744 [0.735, 0.739]	0.747 † [0.735, 0.739]	0.743 [0.735, 0.739]	0.747 † [0.735, 0.739]	0.685 [0.735, 0.739]	0.683 [0.735, 0.739]	0.673 [0.735, 0.739]	0.677 [0.735, 0.739]
ROUGE-WE-1	38.9 [38.4, 39.3]	49.2 [48.8, 49.6]	52.5 [52.0, 52.9]	52.3 [51.9, 52.8]	54.4 † [54.0, 54.8]	54.4 † [54.0, 54.8]	54.0 [53.6, 54.4]	54.8 * [54.4, 55.2]	42.2 [41.8, 42.5]	43.2 [42.8, 43.5]	38.1 [37.8, 38.4]	38.9 [38.6, 39.3]
ROUGE-1	37.8 [37.4, 38.2]	48.4 [48.0, 48.7]	51.9 [51.5, 52.4]	51.8 [51.3, 52.2]	53.8 † [53.4, 54.2]	53.7 † [53.3, 54.1]	53.2 [52.8, 53.6]	54.1 * [53.7, 54.5]	41.6 [41.3, 42.0]	42.6 [42.2, 42.9]	38.4 [38.1, 38.8]	39.2 [38.8, 39.6]
ROUGE-L	28.7 [28.3, 29.1]	35.9 [35.5, 36.4]	38.6 [38.1, 39.1]	38.9 [38.4, 39.4]	40.0 † [39.6, 40.5]	40.3 * [39.9, 40.8]	39.4 [39.0, 39.9]	40.2 † [39.7, 40.7]	28.7 [28.4, 29.1]	28.3 [27.9, 28.7]	27.2 [26.9, 27.6]	28.0 [27.6, 28.3]
ROUGE-LSUM	35.4 [34.9, 35.8]	45.1 [44.7, 45.5]	48.7 [48.2, 49.1]	48.6 [48.2, 49.1]	50.5 † [50.0, 50.9]	50.4 † [49.9, 50.8]	49.8 [49.4, 50.2]	50.8 * [50.4, 51.2]	38.3 [38.0, 38.7]	39.2 [38.9, 39.6]	35.4 [35.0, 35.7]	36.0 [35.7, 36.4]
ROUGE-WE-2	25.6 [25.2, 26.0]	35.6 [35.2, 36.0]	38.8 [38.4, 39.3]	38.6 [38.1, 39.0]	40.3 † [39.8, 40.7]	40.2 † [39.8, 40.7]	39.9 [39.4, 40.3]	40.7 * [40.2, 41.1]	26.8 [26.4, 27.1]	27.6 [27.2, 27.9]	22.7 [22.4, 23.0]	23.5 [23.2, 23.9]
METEOR	0.180 [0.177, 0.182]	0.232 [0.229, 0.235]	0.267 [0.264, 0.270]	0.262 [0.259, 0.265]	0.276 * [0.273, 0.279]	0.272 [0.269, 0.275]	0.272 [0.269, 0.275]	0.279 † [0.276, 0.281]	0.195 [0.192, 0.197]	0.213 [0.211, 0.215]	0.169 [0.167, 0.171]	0.172 [0.170, 0.174]
ROUGE-WE-3	26.5 [26.1, 26.9]	37.2 [36.8, 37.7]	40.8 [40.3, 41.3]	40.5 [40.0, 41.0]	42.3 † [41.8, 42.7]	42.1 † [41.6, 42.5]	41.6 [41.1, 42.0]	42.5 * [42.0, 43.0]	28.3 [27.9, 28.7]	29.4 [29.1, 29.8]	22.9 [22.5, 23.2]	24.0 [23.6, 24.4]
RadGraph	0.225 [0.221, 0.230]	0.348 [0.343, 0.352]	0.381 [0.376, 0.386]	0.383 [0.378, 0.388]	0.395 † [0.390, 0.400]	0.388 [0.383, 0.393]	0.393 † [0.388, 0.398]	0.397 * [0.392, 0.402]	0.221 [0.217, 0.225]	0.235 [0.232, 0.239]	0.177 [0.174, 0.180]	0.190 [0.186, 0.193]
ROUGE-2	17.9 [17.5, 18.3]	26.3 [25.9, 26.8]	29.6 [29.1, 30.0]	29.4 [29.0, 29.9]	30.9 * [30.5, 31.4]	30.7 † [30.2, 31.1]	30.1 [29.6, 30.5]	30.9 † [30.4, 31.4]	15.9 [15.6, 16.2]	16.1 [15.8, 16.4]	13.4 [13.1, 13.6]	13.9 [13.6, 14.2]
PRISM	-3.96 [-3.98, -3.94]	-3.40 [-3.42, -3.37]	-3.34 [-3.37, -3.32]	-3.29 [-3.32, -3.27]	-3.26 † [-3.28, -3.24]	-3.24 † [-3.26, -3.22]	-3.29 [-3.31, -3.26]	-3.26 † [-3.28, -3.24]	-3.99 [-4.01, -3.97]	-4.02 [-4.05, -4.00]	-4.07 [-4.09, -4.05]	-4.07 [-4.09, -4.05]
ROUGE-3	10.3 [10.0, 10.7]	16.5 [16.1, 17.0]	19.3 [18.9, 19.8]	19.4 [18.9, 19.8]	20.5 * [20.1, 21.0]	20.2 † [19.7, 20.6]	19.7 [19.3, 20.2]	20.4 † [19.9, 20.8]	6.8 [6.5, 7.1]	6.7 [6.5, 7.0]	5.2 [5.0, 5.4]	5.5 [5.3, 5.7]
S ³ -pyr	0.37 [0.37, 0.38]	0.58 [0.57, 0.58]	0.70 † [0.69, 0.71]	0.66 [0.65, 0.67]	0.70 † [0.69, 0.71]	0.68 [0.67, 0.69]	0.68 [0.67, 0.69]	0.71 † [0.70, 0.71]	0.44 [0.43, 0.45]	0.52 [0.51, 0.52]	0.36 [0.35, 0.36]	0.37 [0.36, 0.37]
S ³ -resp	0.51 [0.50, 0.52]	0.67 [0.67, 0.68]	0.78 † [0.77, 0.79]	0.75 [0.74, 0.76]	0.78 † [0.77, 0.79]	0.77 [0.76, 0.77]	0.76 [0.76, 0.77]	0.79 * [0.78, 0.79]	0.53 [0.53, 0.54]	0.58 [0.58, 0.59]	0.48 [0.47, 0.48]	0.49 [0.48, 0.49]
Stats-novel trigram	0.85 [0.84, 0.85]	0.76 [0.76, 0.77]	0.68 [0.68, 0.69]	0.69 [0.68, 0.69]	0.62 [0.61, 0.62]	0.68 [0.68, 0.69]	0.65 [0.64, 0.65]	0.65 [0.65, 0.66]	0.98 [0.98, 0.98]	0.99 † [0.99, 0.99]	0.99 * [0.99, 0.99]	0.99 † [0.99, 0.99]
Stats-density	1.89 [1.85, 1.92]	2.98 [2.92, 3.04]	5.43 [5.27, 5.59]	5.49 [5.32, 5.66]	6.51 * [6.34, 6.68]	4.64 [4.53, 4.76]	5.45 [5.31, 5.58]	5.47 [5.33, 5.61]	0.87 [0.86, 0.88]	0.85 [0.85, 0.86]	0.77 [0.77, 0.78]	0.78 [0.77, 0.79]
CIDEr	0.179 [0.159, 0.199]	0.445 [0.411, 0.479]	0.556 [0.517, 0.594]	0.546 [0.507, 0.584]	0.637 * [0.597, 0.677]	0.599 † [0.560, 0.639]	0.600 † [0.561, 0.640]	0.631 † [0.591, 0.671]	0.184 [0.166, 0.202]	0.203 [0.182, 0.224]	0.125 [0.113, 0.137]	0.152 [0.136, 0.167]
BLANC	0.049 [0.047, 0.051]	0.089 [0.086, 0.091]	0.122 [0.119, 0.124]	0.113 [0.111, 0.116]	0.131 * [0.128, 0.134]	0.114 [0.112, 0.117]	0.126 [0.123, 0.128]	0.126 [0.123, 0.129]	0.053 [0.051, 0.054]	0.061 [0.059, 0.063]	0.045 [0.043, 0.047]	0.044 [0.042, 0.046]
Stats-compression	8.36 * [8.20, 8.52]	6.16 [6.04, 6.28]	5.31 [5.18, 5.44]	5.51 [5.40, 5.62]	5.49 [5.37, 5.61]	5.78 [5.66, 5.90]	5.52 [5.41, 5.63]	5.50 [5.37, 5.63]	6.17 [6.02, 6.32]	4.92 [4.78, 5.05]	7.16 [7.00, 7.32]	7.23 [7.08, 7.39]
SUPERT	0.511 [0.509, 0.514]	0.536 [0.533, 0.539]	0.551 [0.548, 0.554]	0.548 [0.545, 0.551]	0.557 * [0.554, 0.560]	0.550 [0.547, 0.553]	0.554 † [0.551, 0.557]	0.553 [0.551, 0.556]	0.512 [0.510, 0.514]	0.521 [0.519, 0.523]	0.506 [0.504, 0.509]	0.504 [0.502, 0.506]
Stats-coverage	0.62 [0.62, 0.63]	0.66 [0.66, 0.66]	0.70 [0.69, 0.70]	0.69 [0.69, 0.70]	0.72 * [0.72, 0.72]	0.70 [0.69, 0.70]	0.71 [0.71, 0.72]	0.71 [0.71, 0.72]	0.56 [0.56, 0.56]	0.57 [0.56, 0.57]	0.54 [0.54, 0.54]	0.54 [0.53, 0.54]
SummaQA	0.063 [0.055, 0.071]	0.089 [0.079, 0.099]	0.168 † [0.151, 0.184]	0.156 [0.141, 0.172]	0.180 * [0.164, 0.196]	0.129 [0.117, 0.142]	0.168 † [0.150, 0.187]	0.166 † [0.151, 0.181]	0.055 [0.048, 0.062]	0.052 [0.044, 0.060]	0.043 [0.036, 0.050]	0.038 [0.033, 0.044]

Note that data are shown as mean [2.5th percentile, 97.5th percentile]. “*” denotes the highest value for each metric, and “†” denotes the values that do not have statistically significant difference (P>0.05) with the highest value.

Figure E3: Assessment of 12 language models using all evaluation metrics included in this study. Displayed numbers are actual metric values, and the 95% confidence intervals were determined via bootstrap resampling.

Appendix S8: Findings and Background Information for the Examples in Expert Evaluation

Figures E4, E5, E6 and E7 show the findings sections associated with Cases 1, 2, 3, 4, in Figure 5 (in the main body), respectively.

Indication: [AGE]-year-old [SEX] with pulmonary nodule, presents for a staging FDG PET/CT examination.	
Findings: Background liver metabolic activity (SUV mean/ SUV max): 3.9/5.7 (PET/CT axial slice 155). Background mediastinal blood pool metabolic activity (SUV mean/ SUV max): 3.1/3.9 (PET/CT axial slice 119). Head/Neck: No FDG avid cervical nodes are noted. Physiologic symmetric FDG uptake is present in the visualized portions of the brain, extraocular muscles, and salivary glands with no distinct focal abnormalities. Chest: Redemonstration of a subpleural oval-shaped solid nodule within the anteroinferior right upper lobe immediately superior to the right minor fissure, measuring approximately 1.2 x 1.3 cm in size, unchanged compared to [DATE]. This has mild associated FDG uptake (SUV max 1.8, axial slice 125). With reference to outside prior CT, there is suggestion of macroscopic fat within the nodule. No other pulmonary nodules are identified. No pleural effusion. No FDG avid lymph nodes are noted in the axillae, hila, or mediastinum. Physiologic FDG uptake is present within the myocardium. No pericardial effusion. Mild calcified atherosclerotic plaque along the aortic arch and at the origins of the great vessels. Redemonstration of a mildly lobulated nodular area of soft tissue within the subareolar right breast. This measures approximately 1.2 x 1.1 cm in size, unchanged compared to [DATE]. This does not appear to have associated FDG uptake. Abdomen/Pelvis: No FDG avid nodes or mesenteric lesions are noted. Heterogeneous FDG uptake is noted in the liver and spleen without focal abnormalities. The adrenal glands appear unremarkable. Mild uptake is noted along the bowel within the normal physiologic variation. Excreted radiotracer is present within the urinary collecting system and bladder. No hydronephrosis. Normal caliber abdominal aorta, with moderate calcified atherosclerotic plaque. Musculoskeletal/Extremities: No FDG avid skeletal lesions are noted. Infiltrated radiotracer is noted within the skeletal right upper arm antecubital region. There are no other areas of abnormal hypermetabolism within the visualized portions of the extremities.	
Original clinical impression [1] FDG PET/CT demonstrates short-term stability of the solitary nodule within the right upper lobe, which has only minimal associated FDG uptake, not elevated above mediastinal blood pool. Given the lack of significant FDG avidity, and the suggestion of macroscopic fat within the nodule on prior diagnostic chest CT, a benign lesion such as a pulmonary hamartoma is a consideration. Could consider short-term follow-up diagnostic CT chest in 3-6 months to assess for interval change. [2] No evidence of suspected FDG avid local nodal mediastinal/hilar or distant metastatic disease. [3] Mildly lobulated nodular soft tissue in the subareolar right breast, without significant FDG avidity. Could correlate with prior mammography, if available. If not, screening mammography is recommended.	PEGASUS-generated impression [1] FDG PET/CT demonstrates a 1.2 x 1.3 cm subpleural solid nodule within the anteroinferior right upper lobe with mild associated FDG uptake, which is nonspecific by PET criteria for an infectious/inflammatory process versus low-grade primary lung malignancy. Recommend correlation with prior and/or follow-up thoracic CT to assess for interval change in size. [2] No evidence of FDG avid local nodal mediastinal/hilar or distant metastatic disease. [3] Redemonstration of a mildly lobulated nodular area of soft tissue within the subareolar right breast, unchanged compared to [DATE]. This does not appear to have associated hypermetabolic activity.

Figure E4: The findings section and relevant background information for Case 1 in Figure 5 (in the main body).

Indication: [AGE] years old patient with history of mantle cell lymphoma diagnosed by left axillary lymph node biopsy. Status post 3 cycles chemotherapy. Patient also has history of right breast lobular carcinoma in situ and ALH in [DATE] status post partial mastectomy and tamoxifen x5 years. Patient is referred for assessment of response to treatment.	
Findings: Physiologic background liver standardized uptake value (SUV mean and SUV max) reported for comparison between PET studies: 2.0 and 2.5, previously 2.3 and 2.9. Visualized head/neck: Physiologic uptake in the visualized portions of the brain, extraocular muscles, and salivary glands. Decreased homogeneous uptake in the thyroid, right thyroid lobe SUV max 2.2, previously SUV max 5.0. Head/neck lymph nodes: Interval resolution of previously noted hypermetabolic bilateral cervical lymphadenopathy. Currently there are few scattered subcentimeter lymph nodes that are not avid. No new suspicious head/neck lymph nodes. Lungs: No lung nodules or abnormal uptake. Mild dependent atelectasis. Pleura/pericardium: No pleural or pericardial effusion. Thoracic lymph nodes: Decreased size and resolved uptake of mediastinal and axillary lymph nodes. For example: -Left axillary lymph node 0.4 x 0.6 cm SUV max 0.8 (axial PET/CT slice 83), previously 1.2 x 0.8 cm SUV max 5.9 -Retrocrural lymph node 0.9 x 0.3 cm SUV max 1.6 (axial PET/CT slice 124), previously 1.5 x 0.7 cm SUV max 5.2. Other chest findings: Physiologic myocardial uptake. Prior right breast lumpectomy. Hepatobiliary: No abnormal uptake. Spleen: Resolved splenomegaly and uptake measuring 9.8 cm in AP dimension SUV max 2.1, previously 22.1 cm SUV max 9.9. Pancreas: No abnormal uptake. Adrenals: Within normal limits. Kidneys/bladder: No abnormal uptake. Physiologically excreted tracer activity within the renal collecting system and urinary bladder. Bowel/peritoneum: No suspicious bowel uptake or abnormality. Diverticulosis without evidence of diverticulitis. Pelvic organs: No abnormal uptake. Uterus is surgically absent. Abdominopelvic lymph nodes: Decreased size and resolved uptake of multiple abdominopelvic lymph nodes. No new suspicious lymph nodes. Musculoskeletal/soft tissues/skin: Decreased heterogeneous marrow uptake. A focus of relatively increased uptake at the T12 endplate without likely corresponds to degenerative changes. No suspicious osseous lesions. Other: None.	
Original clinical impression [1] FDG PET/CT demonstrates interval resolution of multiple bilateral head/neck, thoracic, and abdominopelvic lymph nodes as well as resolved splenomegaly and intense splenic uptake consistent with complete metabolic response. Deauville 1. [2] No new sites of lymphomatous involvement.	PEGASUS-generated impression [1] FDG PET/CT demonstrates interval resolution of previously noted hypermetabolic lymphadenopathy in the neck, chest, abdomen, and pelvis consistent with complete metabolic response (Deauville score 1). [2] Decreased homogeneous uptake in the thyroid.

Figure E5: The findings section and relevant background information for Case 2 in Figure 5 (in the main body).

<p>Indication: Patient is a [AGE]-year-old [SEX] with stage IIIB Merkel cell carcinoma of the left eyebrow status post wide local excision with split-thickness skin graft, left superficial parotidectomy with facial nerve dissection and selective neck dissection levels 2A and 2B on [DATE]. This was followed by adjuvant radiation to the parotid bed, periparotid nodes, and cervical levels 2-4 completed in [DATE]. The purpose of the study is restaging of the disease.</p>	
<p>Findings:</p> <p>Mediastinal blood pool demonstrates mean SUV of 2.2 measured within the descending thoracic aorta at the level of the carina (axial PET/CT image 140); previously 2.3. Background liver demonstrates mean SUV of 2.6 measured within the inferior right hepatic lobe (axial PET/CT image 208); previously 2.7.</p> <p>Head/neck: Note is made of slight interval increase in size and FDG uptake of a mildly hypermetabolic subcutaneous soft tissue nodule within the left neck anterior to the sternocleidomastoid muscle at the level of the thyroid cartilage. It appears more rounded and discrete on the current exam measuring approximately 1.2 cm with SUV max of 2.3 (axial PET/CT image 105) compared with previously 0.9 cm with SUV max of 1.6. Symmetric FDG uptake is present in the visualized portions of the brain, extraocular muscles, larynx, and salivary glands with no distinct focal abnormalities. No new or enlarging FDG-avid cervical lymphadenopathy is noted. Postsurgical changes of left neck dissection are stable with no evidence of suspicious FDG uptake. Oral cavity, oropharynx, nasopharynx, and larynx appear unremarkable. Thyroid gland is diminutive in appearance which is compatible with patient's history of hypothyroidism. Parotid and submandibular glands are unremarkable. Paranasal sinuses are well-aerated. Mastoid air cells and tympanic cavities are clear. No significant dental abnormalities are noted.</p> <p>Chest: No new or enlarging FDG-nodules. No pleural effusion or pneumothorax. Central airways are widely patent. No new or enlarging FDG-avid axillary, mediastinal, or hilar lymphadenopathy is noted. Heart is mildly enlarged in size. Physiological FDG uptake is present within the myocardium. No pericardial effusion. Thoracic aorta is normal in course and caliber. Mild atheromatous calcifications are present in the thoracic aorta and left anterior descending coronary artery.</p> <p>Abdomen/Pelvis: Expected physiologic FDG uptake is noted within the solid and hollow abdominopelvic viscera. Non-FDG avid high-attenuation cysts in both kidneys are stable and may be proteinaceous or hemorrhagic in nature. Representative lesion at the superior pole of the left kidney measures 2.0 cm in size and 1.5 cm upper pole right kidney. Photopenic 5-mm simple cyst in the interpolar region of the right kidney. Tiny nonobstructing calculus is noted in the right kidney. There is sigmoid diverticulosis without CT-evidence of diverticulitis. Surgical absence of the uterus. Excreted radiotracer is present within the urinary collecting system and bladder. Right ureter is mildly prominent unchanged from before. No FDG-avid abdominopelvic lymphadenopathy is noted. Atherosclerotic calcifications are present in the nonaneurysmal abdominal aorta and iliac arteries.</p> <p>Musculoskeletal: No suspicious FDG uptake is noted in the region of the left eyebrow when compared to PET/PET dated [DATE]. No suspicious FDG uptake is noted elsewhere in the skin or muscle or bone. Degenerative disc and facet disease is noted in the spine with diffuse demineralization. Superficial venous collaterals are noted in bilateral lower extremities.</p>	
<p>Original clinical impression</p> <p>[1] Slight interval increase in size and FDG uptake of a mildly hypermetabolic subcutaneous soft tissue nodule in the left neck anterior to the sternocleidomastoid muscle which appears more rounded and discrete on the current exam when compared to most recent PET/CT from [DATE]. This finding possibly represents metastatic disease but not particularly avid. Recommend ultrasound-guided sampling for biopsy confirmation.</p> <p>[2] No abnormal FDG uptake to suggest FDG-avid locally recurrent or additional sites of metastatic disease.</p> <p>[3] Probable proteinaceous/hemorrhagic renal cysts. Recommend confirmation with ultrasound.</p>	<p>PEGASUS-generated impression</p> <p>[1] Slight interval increase in size and FDG uptake of a mildly hypermetabolic subcutaneous soft tissue nodule within the left neck anterior to the sternocleidomastoid muscle at the level of the thyroid cartilage is favored to represent post therapeutic inflammation rather than recurrent disease. Recommend attention on follow-up.</p> <p>[2] No evidence of FDG-avid local or distant metastatic disease.</p>

Figure E6: The findings section and relevant background information for Case 3 in Figure 5 (in the main body).

<p>Indication: [AGE]-year-old [SEX] with history of invasive ductal carcinoma of the left breast. Left axillary lymphadenopathy seen on initial staging. Also with concern for osseous metastatic disease in the pelvis, left clavicle, and lumbar spine. At the end of 2018 progressive disease was seen in the axilla. Currently treated with Fulvestrant (with Palbociclib) and Zometa. Most recent imaging with some suspicious nodular tissue posterior to the left breast clip as well as enlarging left axillary lymphadenopathy ([DATE]). Request to evaluate for disease status.</p>	
<p>Findings:</p> <p>Background liver metabolic activity (SUV mean/ SUV max): 3.0/3.9 (PET/CT axial slice 158); Background mediastinal blood pool metabolic activity (SUV mean/ SUV max): 2.4/2.7 (PET/CT axial slice 113);</p> <p>Skull base/Neck: No FDG avid cervical nodes are noted. There is moderate FDG activity associated with the eyelids bilaterally. Additionally there is some mild-moderate activity associated with the nasal mucosa which may represent mild nonspecific inflammation. Physiologic symmetric FDG uptake is present in the visualized portions of the brain, extraocular muscles, and salivary glands with no distinct focal abnormalities. Likely meningioma near the falx in the right frontal region. Paranasal sinuses are free of significant disease. Tympanic and mastoid air cells clear.</p> <p>Chest: Redemonstration of left axillary lymphadenopathy which demonstrates moderate-intense FDG avidity. Overall these appear similar in size and distribution compared to [DATE]. For example a posterior axillary lymph node measures 11 mm (PET/CT axial slice 109; SUV max 13.2) compared to 11 mm previously. A lower axillary lymph node measures 13 mm (PET/CT/CT axial slice 122; SUV max 6.0) compared to 14 mm previously. The area of nodular soft tissue at the posterior aspect of the left breast glandular tissue, near the biopsy clip, which appear to be enlarging on previous CT examinations demonstrates intense FDG avidity (SUV max 13.8; PET/CT axial slice 134). The area of FDG avidity measures approximately 2.7 x 3.5 x 3.9 cm (LR-AP-CC) in maximal dimension. No FDG avid lung nodules are noted. Physiologic FDG uptake is present within the myocardium. Unchanged heart size. No pericardial or pleural effusion. No pneumothorax. Dependent atelectasis. Calcified hilar and subcarinal lymphadenopathy suggestive of prior granulomatous infection.</p> <p>Abdomen/Pelvis: There is slight misregistration, especially in the upper abdomen, due to patient motion. No FDG avid nodes or mesenteric lesions are noted. Heterogeneous FDG uptake is noted in the liver and spleen without focal abnormalities. The adrenal glands appear unremarkable. Moderate uptake is noted along the bowel. There is no corresponding focal CT abnormality seen. Excreted radiotracer is present within the urinary collecting system and bladder. The unenhanced contours of the liver, spleen, adrenal glands, pancreas are within normal limits. The gallbladder is surgically absent. Unchanged mild dilatation of the extrahepatic bile ducts, consistent with reservoir effect. Symmetric renal cortical thickness. No hydronephrosis. No bowel obstruction. Scattered colonic diverticula without CT findings of diverticulitis. Appendix surgically absent. No adnexal masses. No lymphadenopathy in the abdomen or pelvis.</p> <p>Musculoskeletal/Extremities: There is heterogeneous mild FDG activity associated with the osseous pelvis which corresponds to a very mottled sclerotic and lytic appearance. Within the T8 vertebral body there is a small focus of increased FDG avidity (SUV max 3.3; PET/CT axial slice 129) which does not have a clear CT correlate. There is also some heterogeneous mildly increased FDG uptake associated with the lumbar vertebral bodies, nonspecific. There is no definite focal increased FDG uptake associated with the left clavicle which was the site of previously suspected metastatic disease. Elsewhere there is increased uptake associated with the bilateral shoulders, left C2/C3 facet joint, additional intervertebral disk and facet spaces, and the bilateral hips most suggestive of degenerative change.</p>	
<p>Original clinical impression</p> <p>[1] FDG PET/CT demonstrates intense FDG activity associated with the area of nodular soft tissue thickening at the posterior aspect of the left breast, highly suspicious for recurrent/residual malignancy.</p> <p>[2] Intense FDG avidity associated with the left axillary lymphadenopathy, which is overall unchanged in size and distribution compared to the recent [DATE] CT, also highly suspicious for persistent nodal metastatic disease.</p> <p>[3] No definite evidence of FDG avid osseous metastatic disease. Mild heterogeneous FDG activity, similar to normal bone marrow activity, corresponding to mottled sclerotic and lytic changes in the pelvis, lumbar spine and T8 vertebral body, most likely represents physiologic bone marrow activity at sites of previously treated osseous metastatic disease.</p>	<p>PEGASUS-generated impression</p> <p>[1] FDG PET/CT demonstrates intense FDG activity associated with the enlarging nodular soft tissue at the posterior aspect of the left breast glandular tissue, which appears to be enlarging on previous CT examinations. This finding is highly suspicious for recurrent malignancy.</p> <p>[2] Moderate-intense FDG avid left axillary lymphadenopathy, similar in size and distribution compared to recent chest CT from [DATE], compatible with nodal metastatic disease.</p> <p>[3] Heterogeneous mild to moderate FDG uptake associated with sclerotic and lytic osseous changes in the pelvis, left clavicle, and T8 vertebral body, with no definite correlative CT bone abnormality on our corresponding low-dose noncontrast CT. These findings are nonspecific but favored to represent posttreatment related inflammatory change rather than residual/recurrent disease. Recommend attention to these sites on follow-up imaging.</p> <p>[4] No evidence of FDG-avid distant metastatic disease in the chest, abdomen, or pelvis.</p>

Figure E7: The findings section and relevant background information for Case 4 in Figure 5 (in the main body).

Appendix S9: Findings and Background Information for the Examples in Encoding Physician-specific Styles

Figures E8 and E9 show the findings sections associated with Cases 1 and 2 in Figure 6 (in the main body), respectively.

Indication: [AGE]-year-old [SEX] with recently diagnosed poorly adenocarcinoma of the right upper lobe status post biopsy on [DATE]. Patient is referred for initial staging.		
Findings: Physiologic background liver standardized uptake value (SUV mean and SUV max) reported for comparison between PET studies: 2.7 and 3.8. Visualized head/neck: Physiologic uptake in the visualized portions of the brain, extraocular muscles, and salivary glands. Head/neck lymph nodes: No suspicious head/neck lymph nodes. Lungs: Medial right upper lobe apical segment pulmonary nodule abutting the pleura measuring 1.5 x 1.6 cm, SUV max 13.5, axial image 70. No additional nodules. Right middle lobe granuloma. Left lingular atelectasis/scarring. Pleura/pericardium: Mild to moderate FDG activity corresponding same right lower lobe posterior pleural thickening at the 8th/9th intercostal region measuring 0.8 x 0.4 cm, SUV max 3.7, axial image 110, suspicious for a pleural metastatic implant. This focus appears to correspond to subtle oral thickening seen on chest CT from [DATE] (series 3, axial slice 315; series 2, axial slice 79). This focus does not appear to be misregistered PET activity adjacent lung or bone to suggest FDG avid osseous or additional lung metastasis. This focus is less likely to represent top normal physiologic muscle activity. No pleural or pericardial effusion. Thoracic lymph nodes: No suspicious thoracic lymph nodes. Scattered calcified hilar and mediastinal lymph nodes. Other chest findings: Physiologic myocardial uptake. Moderate coronary artery calcifications. Hepatobiliary: No abnormal uptake. Spleen: No abnormal uptake. Pancreas: No abnormal uptake. Adrenals: Non-FDG avid left adrenal gland nodule measuring 1.3 cm, SUV max 2.2, with fat attenuation on noncontrast CT (-18 Hounsfield units). Normal right adrenal gland. Kidneys/bladder: No abnormal uptake. Physiologically excreted tracer activity within the renal collecting system and urinary bladder. Exophytic right and left renal cysts. Bowel/peritoneum: No suspicious bowel uptake or abnormality. Pelvic organs: No abnormal uptake. Abdominopelvic lymph nodes: No suspicious abdominopelvic lymph nodes. Musculoskeletal/soft tissues/skin: Degenerative changes of the spine. No suspicious osseous lesion. Other: None.		
Original clinical impression dictated by Physician 1 [1] FDG PET/CT demonstrates an intensely FDG medial right upper lobe apical pulmonary nodule abutting the pleura, compatible with biopsy-proven primary lung malignancy. [2] Mild to moderate focus of FDG activity in the posterior right lower lobe corresponding to subtle soft tissue pleural thickening at the 8th/9th intercostal region on CT, suspicious for a metastatic pleural implant. [3] No evidence of other sites of FDG avid local nodal or distant metastatic disease. [4] Stable non-FDG left adrenal gland nodule dating to [DATE], most consistent with a benign myelipoma..	PEGASUS-generated impression in Physician 1's style [1] FDG PET/CT demonstrates an intensely FDG avid 1.5 x 1.6 cm right upper lobe apical segment pulmonary nodule, consistent with biopsy-proven primary lung malignancy. [2] Mild to moderate FDG activity corresponding right lower lobe posterior pleural thickening at the 8th/9th intercostal region, suspicious for a pleural metastatic implant. [3] No evidence of other sites of suspected PET avid local nodal or distant metastatic disease. [4] Non-FDG avid 1.3 cm left adrenal nodule, with fat attenuation on noncontrast CT, which is indeterminate. Recommend adrenal protocol CT or MRI for further evaluation.	PEGASUS-generated impression in Physician 2's style [1] Right upper lobe primary lung malignancy with suspected right lower lobe pleural metastasis. [2] No evidence of nodal or distant metastases. [3] Indeterminate left adrenal nodule can be followed on future surveillance imaging.

Figure E8: The findings section and relevant background information for Case 1 in Figure 6 (in the main body).

Indication: [AGE] year old [SEX] with new diagnosis of right upper lobe nodule biopsy consistent with squamous cell carcinoma. Patient is referred for initial staging.		
Findings: Physiologic background liver standardized uptake value (SUV mean and SUV max) reported for comparison between PET studies: 2.6 and 5.0. Visualized head/neck: Physiologic uptake in the visualized portions of the brain, extraocular muscles, and salivary glands. Head/neck lymph nodes: No suspicious head/neck lymph nodes. Lungs: Avid right upper lobe mass is consistent with biopsy-proven primary lung malignancy, 3.0 x 2.4 cm, SUV max 7.5 (series 1200 image 89). Other lung findings are better evaluated on recent dedicated chest CT. No other abnormal uptake. Emphysema. Pleura/pericardium: No pleural or pericardial effusion. Thoracic lymph nodes: No suspicious thoracic lymph nodes. Uptake of the mediastinal lymph nodes is probably reactive/inflammatory. Other chest findings: Coronary vascular and scattered thoracic aortic calcification. Bilateral gynecomastia. Benign incidental tracheal diverticulum. Hepatobiliary: No abnormal uptake. Prior liver transplant. Fatty liver. Cholecystectomy. Spleen: No abnormal uptake. Pancreas: No abnormal uptake. Adrenals: Within normal limits. Kidneys/bladder: No abnormal uptake. Physiologically excreted tracer activity within the renal collecting system and urinary bladder. Bowel/peritoneum: No suspicious bowel uptake or abnormality. Diverticulosis without inflammatory change. Pelvic organs: No abnormal uptake. Abdominopelvic lymph nodes: No suspicious abdominopelvic lymph nodes. Musculoskeletal/soft tissues/skin: No suspicious osseous lesions. Diffuse marrow uptake is probably reactive and benign. Multilevel spine DJD. Prior lumbar laminectomy. Reactive uptake near the left greater trochanter. Other: Aortoiliac atherosclerotic vascular calcifications. Small umbilical hernia."		
Original clinical impression dictated by Physician 2 Primary right upper lobe lung malignancy without evidence for nodal or distant metastases.	PEGASUS-generated impression in Physician 1's style [1] FDG PET/CT demonstrates an intensely FDG avid right upper lobe mass consistent with biopsy-proven primary lung malignancy. [2] No evidence of other sites of abnormal FDG uptake to suggest locoregional or distant metastatic disease.	PEGASUS-generated impression in Physician 2's style Right upper lobe primary lung malignancy without evidence of nodal or distant metastases.

Figure E9: The findings section and relevant background information for Case 2 in Figure 6 (in the main body).

Reference

1. Zhang Y, Ding DY, Qian T, Manning CD, Langlotz CP. Learning to Summarize Radiology Findings. Proc Ninth Int Workshop Health Text Min Inf Anal. Brussels, Belgium: Association for Computational Linguistics; 2018. p. 204–213. doi: 10.18653/v1/W18-5623.
2. Chen C, Yin Y, Shang L, et al. bert2BERT: Towards Reusable Pretrained Language Models. Proc 60th Annu Meet Assoc Comput Linguist Vol 1 Long Pap. Dublin, Ireland: Association for Computational Linguistics; 2022. p. 2134–2148. doi: 10.18653/v1/2022.acl-long.151.
3. Li Y, Wehbe RM, Ahmad FS, Wang H, Luo Y. Clinical-Longformer and Clinical-BigBird: Transformers for long clinical sequences. arXiv; 2022. <http://arxiv.org/abs/2201.11838>. Accessed August 16, 2023.
4. Liu Y, Ott M, Goyal N, et al. RoBERTa: A Robustly Optimized BERT Pretraining Approach. arXiv; 2019. <http://arxiv.org/abs/1907.11692>. Accessed August 16, 2023.
5. Lewis M, Liu Y, Goyal N, et al. BART: Denoising Sequence-to-Sequence Pre-training for Natural Language Generation, Translation, and Comprehension. arXiv; 2019. <http://arxiv.org/abs/1910.13461>. Accessed March 7, 2023.
6. Yuan H, Yuan Z, Gan R, Zhang J, Xie Y, Yu S. BioBART: Pretraining and Evaluation of A Biomedical Generative Language Model. arXiv; 2022. <http://arxiv.org/abs/2204.03905>. Accessed August 15, 2023.
7. Zhang J, Zhao Y, Saleh M, Liu PJ. PEGASUS: Pre-training with Extracted Gap-sentences for Abstractive Summarization. arXiv; 2020. <http://arxiv.org/abs/1912.08777>. Accessed March 7, 2023.
8. Raffel C, Shazeer N, Roberts A, et al. Exploring the Limits of Transfer Learning with a Unified Text-to-Text Transformer. arXiv; 2020. <http://arxiv.org/abs/1910.10683>. Accessed August 14, 2023.
9. Lu Q, Dou D, Nguyen TH. ClinicalT5: A Generative Language Model for Clinical Text. Findings of the Association for Computational Linguistics: EMNLP 2022, pages 5436–5443, Abu Dhabi, United Arab Emirates. Association for Computational Linguistics. doi: 10.18653/v1/2022.findings-emnlp.398.
10. Johnson AEW, Pollard TJ, Berkowitz SJ, et al. MIMIC-CXR, a de-identified publicly available database of chest radiographs with free-text reports. Sci Data. 2019;6(1):317. doi: 10.1038/s41597-019-0322-0.
11. Wei J, Bosma M, Zhao VY, et al. Finetuned Language Models Are Zero-Shot Learners. arXiv; 2022. <http://arxiv.org/abs/2109.01652>. Accessed August 15, 2023.
12. Ziegler DM, Stiennon N, Wu J, et al. Fine-Tuning Language Models from Human Preferences. arXiv; 2020. <http://arxiv.org/abs/1909.08593>. Accessed August 14, 2023.
13. Zhang S, Roller S, Goyal N, et al. OPT: Open Pre-trained Transformer Language Models. arXiv; 2022. <http://arxiv.org/abs/2205.01068>. Accessed February 22, 2023.
14. Touvron H, Lavril T, Izacard G, et al. LLaMA: Open and Efficient Foundation Language Models. arXiv; 2023. <http://arxiv.org/abs/2302.13971>. Accessed August 14, 2023.
15. Hu EJ, Shen Y, Wallis P, et al. LoRA: Low-Rank Adaptation of Large Language Models. arXiv; 2021. <http://arxiv.org/abs/2106.09685>. Accessed August 15, 2023.

16. Taori R, Gulrajani I, Zhang T, et al. Stanford Alpaca: An Instruction-following LLaMA model. GitHub; 2023. https://github.com/tatsu-lab/stanford_alpaca. Accessed June 20, 2023.
17. Loshchilov I, Hutter F. Decoupled Weight Decay Regularization. arXiv; 2019. <http://arxiv.org/abs/1711.05101>. Accessed August 31, 2023.
18. Lin CY. ROUGE: A package for automatic evaluation of summaries. In Text Summarization Branches Out, Barcelona, Spain, July 2004. Association for Computational Linguistics, 2004; 74–81. <https://aclanthology.org/W04-1013/>.
19. Papineni K, Roukos S, Ward T, Zhu W-J. BLEU: a method for automatic evaluation of machine translation. Proc 40th Annu Meet Assoc Comput Linguist - ACL 02. Philadelphia, Pennsylvania: Association for Computational Linguistics; 2001. p. 311. doi: 10.3115/1073083.1073135.
20. Popović M. chrF: character n-gram F-score for automatic MT evaluation. Proc Tenth Workshop Stat Mach Transl. Lisbon, Portugal: Association for Computational Linguistics; 2015. p. 392–395. doi: 10.18653/v1/W15-3049.
21. Banerjee, S. and Lavie, A. METEOR: An Automatic Metric for MT Evaluation with Improved Correlation with Human Judgments. Proceedings of Workshop on Intrinsic and Extrinsic Evaluation Measures for MT and/or Summarization. Ann Arbor, Michigan: Association of Computational Linguistics, 2005. p. 65–72.
22. Vedantam R, Zitnick CL, Parikh D. CIDEr: Consensus-based Image Description Evaluation. arXiv; 2015. <http://arxiv.org/abs/1411.5726>. Accessed August 31, 2023.
23. Ng J-P, Abrecht V. Better Summarization Evaluation with Word Embeddings for ROUGE. arXiv; 2015. <http://arxiv.org/abs/1508.06034>. Accessed August 31, 2023.
24. Zhang T, Kishore V, Wu F, Weinberger KQ, Artzi Y. BERTScore: Evaluating Text Generation with BERT. arXiv; 2020. <http://arxiv.org/abs/1904.09675>. Accessed August 22, 2023.
25. Zhao W, Peyrard M, Liu F, Gao Y, Meyer CM, Eger S. MoverScore: Text Generation Evaluating with Contextualized Embeddings and Earth Mover Distance. Proc 2019 Conf Empir Methods Nat Lang Process 9th Int Jt Conf Nat Lang Process EMNLP-IJCNLP. Hong Kong, China: Association for Computational Linguistics; 2019. p. 563–578. doi: 10.18653/v1/D19-1053.
26. Hu J, Li J, Chen Z, et al. Word Graph Guided Summarization for Radiology Findings. arXiv; 2021. <http://arxiv.org/abs/2112.09925>. Accessed March 2, 2023.
27. Yuan W, Neubig G, Liu P. BARTScore: Evaluating Generated Text as Text Generation. arXiv; 2021. <http://arxiv.org/abs/2106.11520>. Accessed August 15, 2023.
28. Thompson B, Post M. Automatic Machine Translation Evaluation in Many Languages via Zero-Shot Paraphrasing. Proc 2020 Conf Empir Methods Nat Lang Process EMNLP. Online: Association for Computational Linguistics; 2020. p. 90–121. doi: 10.18653/v1/2020.emnlp-main.8.
29. Peyrard M, Botschen T, Gurevych I. Learning to Score System Summaries for Better Content Selection Evaluation. Proc Workshop New Front Summ. Copenhagen, Denmark: Association for Computational Linguistics; 2017. p. 74–84. doi: 10.18653/v1/W17-4510.
30. Zhong M, Liu Y, Yin D, et al. Towards a Unified Multi-Dimensional Evaluator for Text Generation. Proc 2022 Conf Empir Methods Nat Lang Process. Abu Dhabi, United Arab Emirates: Association for Computational Linguistics; 2022. p. 2023–2038. doi: 10.18653/v1/2022.emnlp-main.131.

31. Scialom T, Lamprier S, Piwowarski B, Staiano J. Answers Unite! Unsupervised Metrics for Reinforced Summarization Models. arXiv; 2019. <http://arxiv.org/abs/1909.01610>. Accessed August 31, 2023.
32. Lita LV, Rogati M, Lavie A. BLANC: learning evaluation metrics for MT. Proc Conf Hum Lang Technol Empir Methods Nat Lang Process - HLT 05. Vancouver, British Columbia, Canada: Association for Computational Linguistics; 2005. p. 740–747. doi: 10.3115/1220575.1220668.
33. Gao Y, Zhao W, Eger S. SUPERT: Towards New Frontiers in Unsupervised Evaluation Metrics for Multi-Document Summarization. Proc 58th Annu Meet Assoc Comput Linguist. Online: Association for Computational Linguistics; 2020. p. 1347–1354. doi: 10.18653/v1/2020.acl-main.124.
34. Grusky M, Naaman M, Artzi Y. Newsroom: A Dataset of 1.3 Million Summaries with Diverse Extractive Strategies. Proc 2018 Conf North Am Chapter Assoc Comput Linguist Hum Lang Technol Vol 1 Long Pap. New Orleans, Louisiana: Association for Computational Linguistics; 2018. p. 708–719. doi: 10.18653/v1/N18-1065.
35. Fabbri AR, Kryściński W, McCann B, Xiong C, Socher R, Radev D. SummEval: Re-evaluating Summarization Evaluation. Trans Assoc Comput Linguist. 2021;9:391–409. doi: 10.1162/tacl_a_00373.
36. Huemann Z, Lee C, Hu J, Cho SY, Bradshaw T. Domain-adapted large language models for classifying nuclear medicine reports. arXiv; 2023. <http://arxiv.org/abs/2303.01258>. Accessed March 17, 2023.